Technical Report

Object-Oriented Vegetation Classification at Peninsular National Parks in California with Airborne High Resolution Imagery: DAIS

Submitted to:

National Park Service
Point Reyes National Seashore
1 Bear Valley Rd.
Point Reyes Station CA 94956

May 20, 2005

By Principal Investigators

Peng Gong

Greg Biging

And team members:

Qian Yu, Nick Clinton

Center for Assessment and Monitoring of Forest and Environmental Resources

College of Natural Resources

137 Mulford Hall - 3110
University of California
Berkeley, CA 94720
(510) 642-5170
(510) 643-5098 fax

ABSTRACT

We conducted vegetation mapping at Point Reyes National Seashore and Golden Gate National Recreation Area in Northern California to create a comprehensive vegetation inventory, covering about 714 km^2 and requiring 48 DAIS frames. Information was stored in a vector database comprised of a series of shape file (one per DAIS frame).

In this project we evaluate the capability of high spatial resolution airborne DAIS (Digital Airborne Imaging System) imagery for detailed vegetation classification at the alliance level with the aid of topographic data. Image objects as minimum classification units were generated through FNEA (Fractal Net Evolution Approach) segmentation using eCognition software. For each object, 52 features were calculated including spectral features, textures, topographic features and geometric features. After statistically ranking the importance of these features with the CART algorithm (classification and regression tree), the most effective features for classification were used to classify the vegetation. Due to the uneven sample size for each class, we chose a non-parametric (nearest neighbor) classifier. We built a hierarchical classification scheme and selected features for each of the broadest categories to carry out the detailed classification, which significantly improved the accuracy. Pixel-based maximum likelihood classification (MLC) with comparable features was used as a benchmark in evaluating our approach. The object-based classification approach overcame the problem of salt-and-pepper effects found in classification results from traditional pixel-based approaches. The method takes advantage of the rich amount of local spatial information present in the irregularly shaped objects in an image. This classification approach was successfully implemented. Computer-assisted classification of high spatial resolution remotely sensed imagery has good potential to substitute or augment the present ground-based inventory of National Park lands.

CONTENTS

LIST OF TABLES

LIST OF FIGURES

INTRODUCTION

North America is facing with a "widespread crisis" due to its shrinking biodiversity, according to a new report by the North American Commission for Environmental Cooperation (CEC). Forested ecosystems in California are undergoing accelerated change due to natural and anthropogenic disturbances (Rogan et al, 2002). As our need increases for ecosystem and larger scale approaches to biodiversity conservation, remote sensing becomes a useful tool to vegetation inventory and monitoring. Remotely sensed data can be used to estimate regional variation in biodiversity, analyze species diversity and richness patterns, and monitor changes in conservation efforts (Mooney and Chapin 1994, Rey-Benayas and Pope 1995, O'Neill et al.1997, Stohlgren et al.1997, Gould 2000). We assess the potential of high spatial resolution airborne remote sensing data in vegetation classification and mapping in the Point Reyes National Seashore (PRNS) and Golden Gate National Recreation Area (GGNRA), so as to provide the information on plant community composition and their spatial distribution.

Remote sensing provides a useful source of data from which updated land cover information can be extracted for assessing and monitoring vegetation changes. In the past several decades, airphoto interpretation has played an important role in detailed vegetation mapping (Sandmann and Lertzman, 2003) in the park lands, which is error-prone and labor intensive due to inconsistencies among interpreters. Traditionally, satellite imagery lacks the level of spatial details for vegetation information extraction in order to spatially inventory and monitor the dynamics of vegetation cover to meet the requirements of conservation management. Applications of coarser spatial resolution satellite imagery such as Landsat Thematic Mapper (TM) and SPOT High Resolution Visible (HRV) alone have often proven insufficient or inadequate for differentiating species-level vegetation in detailed vegetation studies (Kalliola and Syrjanen, 1991; Harvey and Hill, 2001). Classification accuracy is reported to be only 40% or less for thematic information extraction at the species-level with these image types (Czaplewski and Patterson, 2003). Previous studies with multispectral imagery are limited to the differentiation of vegetation density and classification of vegetation types into broad categories such as broadleaf and conifer.

However, high spatial resolution remote sensing is becoming increasingly available; airborne and spaceborne multispectral imagery can be obtained at spatial resolutions at or better

than 1 m. These provide us with new opportunities to test digital image analysis and create new demands to develop new image analysis algorithms for information extraction from high spatial resolution airborne and satellite-borne multispectral imagery. The utility of high spatial resolution for automated vegetation composition classification needs to be evaluated (Ehlers *et al.*, 2003). High spatial resolution imagery for urban-related feature extraction has been used (Jensen and Cowen, 1999; Benediktsson *et al.*, 2003; Herold *et al.*, 2003a). However, there has not been as much work in detailed vegetation mapping using high spatial resolution imagery. This preference for urban areas is partly due to the similarity of the spectral signatures for different species and the difficulties in capturing texture features for vegetation (Carleer and Wolff, 2004).

While high spatial resolution remotely sensed data provide more information than coarse resolution imagery for detailed observation on vegetation, increasingly smaller spatial resolution does not necessarily benefit classification performance and accuracy (Marceau *et al.*, 1990; Gong and Howarth, 1992b; Hay *et al.*, 1996; Hsieh *et al.*, 2001). With the increase in spatial resolution, single pixels no longer capture the characteristics of those heterogeneous categories. The increase in intra-class spectral variability causes a reduction of statistical separability between classes with traditional pixel-based classification approaches. Consequently, classification accuracy is reduced, and the classification results show a salt-and-pepper effect, with individual pixels classified differently from their neighbors. To overcome this so-called H-resolution problem, some pixel-based methods have already been implemented, mainly consisting of three categories: 1) image pre-processing, such as low-pass filter and texture analysis (Gong *et al.*, 1992; Hill and Foody, 1994), 2) contextual classification (Gong and Howarth, 1992a), and 3) post-classification processing, such as mode filtering, morphological filtering, rule-based processing, and probabilistic relaxation (Gong and Howarth, 1989; Shackelford and Davis, 2003; Sun *et al.*, 2003). A common aspect of these methods is that they incorporate spatial information to characterize each class using neighborhood relationships. These techniques can improve classification accuracy considerably. However, they have some disadvantages when applied to high spatial resolution images (1-10m). Firstly, the pre-defined neighborhood window size may not favor all the land cover types evenly since different classes reach their maximum accuracies at different pixel window sizes. Secondly, these techniques require intensive computation especially for high resolution imagery in which the window size should be set relatively large

(Hodgson, 1998). Finally, these processes have blur effects and cannot produce accurate results at the boundaries of different land cover units, although this so-called boundary effect can be reduced with a kernel-based technique (Gong, 1994).

Object-based classification may be a good alternative to the traditional pixel based methods. To overcome the H-resolution problem and salt-and-pepper effect, it is useful to analyze groups of contiguous pixels as objects instead of using the conventional pixel-based classification unit. In theory, this will reduce the local spectral variation caused by crown textures, gaps and shadows. In addition, with spectrally homogeneous segments of images, both spectral values and spatial properties such as size and shape can be explicitly utilized as features for further classification. The basic idea of this process is to group the spatially adjacent pixels into spectrally homogenous objects first and then conduct classification on objects as the minimum processing units. Kettig and Landgrebe (1976) proposed this idea and developed the spectral-spatial classifier called ECHO (extraction and classification of homogeneous objects). More recently, some research has adopted this method on land use or land cover classification combined with image interpretation knowledge and classification results were significantly improved (Gong and Howarth, 1990; Ton *et al.*, 1991; Johnsson, 1994; Hill, 1999; Herold *et al.*, 2003b). As Kettig and Landgrebe pointed out, the premise of this technique is that the objects of interest are large compared to the size of a pixel. Therefore, this approach was not extensively studied or implemented for land cover mapping at the time when TM and HRV data prevailed as readily available multispectral data. An increasing body of research realizes that the object-based approach will be promising for handling high resolution imagery. Hay et al (1996) used a Delaunay triangulation composed of conifer tree tops (local maximum) as image texture primitives and classified each tree top (the nodes of the objects) for airborne CASI NIR data with a spatial resolution of 1.2 m. They demonstrated that this method outperformed the conventional textures. However, it is not feasible to apply this method to broadleaf forest since tree tops cannot be easily identified. Besides this, few studies have been reported to compare the efficiency of an object-based approach with a conventional pixel-based approach for high resolution remote sensing imagery.

There have been successes in the employment of hyperspectal data and multi-temporal data for species classification (Gong *et al.*, 1997; 2001; Dennison and Roberts, 2003; Krishnaswamy *et al.*, 2004). However, the resolution and the data availability of hyperspectal and multi-

temporal data are unsatisfactory. Study on detailed vegetation mapping with widely-used high resolution multispectral imagery is worthwhile even though there are some difficulties. On one hand, spectral features of multispectral imagery are indistinct among different vegetation types (Carleer and Wolff, 2004). On the other hand, the spectral features vary a lot within each type. This is because in high resolution images, each pixel is not closely related to vegetation physiognomy as a whole and vegetation always shows heterogeneity as a result of irregular shadow or shade (Ehlers *et al.*, 2003). In addition to the difficulties in classification, the training sample size for each class may vary due to the uneven distribution of vegetation, budget or practical constraints of training data collection and physical access (Foody, 2002). Facing with all those problems, we propose to use an object-based approach to perform the detailed vegetation classification. The primary objective of our research is to test and evaluate the efficiency of computer-assisted detailed vegetation classification with high resolution remote sensing imagery. We employ an object-based approach in order to make use of the maximum information of high resolution data. We assess the potential of the proposed object-based method with high spatial resolution airborne remote sensing data in vegetation identification and mapping. This work will provide information on plant community composition and their spatial distribution. A nonparametric classifier was adopted for characterization of object primitives and vegetation mapping. The results were compared with those produced by the conventional pixel-based maximum likelihood classifier (MLC).

Considering the large mapping area and the complex vegetation types (classes) in this study, we expect the object-based approach to improve the vegetation classification accuracy through three mechanisms. First, the inclusion of information from ancillary data and intensity-hue-saturation (IHS) transform indices in the classification leads to a more effective vegetation classification. Second, objects are used as the minimum classification unit, which can overcome the H-resolution problem and make better use of the local variance-reduced information of high resolution images for traditional classifiers (Hay *et al.*, 1996; Baatz and Schape, 2000). Finally, the CART algorithm is employed to search for the optimal subset of features in nearest neighbor classification. Feature selection may reduce the number of features given as input to a classifier, while preserving the classification accuracy. Instead of using statistical separability of classes as a selection criterion, we used CART to match the non-parametric nearest neighbor classifier.

SITE DESCRIPTION AND AVAILABLE DATA

Point Reyes National Seashore (PRNS) is located in a peninsular area in Northern California. It was established by President John F.Kennedy on September 13, 1962. Along with the GGNRA, the largest urban national park in the world, over 100,000 acres of open space are preserved. The fauna, flora and geological history of this area are both diverse and unique. Because the Point Reyes is actually located on the Pacific plate, which is separated from the rest of Northern California coastal area on North American plate by the San Andreas Fault, it is significantly different than the adjacent coastal areas. It contains unique elements of biological and historical interest in a spectacularly scenic panorama of thunderous ocean breakers, open grasslands, bushy hillsides and forested ridges. The biological diversity stems from a favorable location in the middle of California and the natural occurrence of many distinct habitats. Nearly 20% of the State's flowering plant species are represented on the peninsula and over 45% of the bird species in North America have been sighted (National Park Service, 2002). With its unique geological, climate and soil conditions, this area supports an unusually high number of rare plant species. Small populations of the twelve rare species, including Coast rock cress, Raven's manzanita, San Francisco spineflower, Franciscan thistle, are scattered throughout the site, in such areas as the Baker Beach sand terraces, the serpentine coastal bluffs and the grasslands extending from Inspiration Point down to El Polin Spring. Meanwhile, the forests are mainly comprised of Monterey cypress, Douglas fir, Bishop pine, Monterey pine, blue gum eucalyptus, blackwood acacia and coast redwood, which serve as important habitats of rare and endangered species. However, many of these trees in the century-old forest are now entering a period of much slower growth toward their lifespan and eventual decline. Breakage and tree mortality could substantially reduce the extent of the forest over the next 20 years. Damage from storms is also expected to accelerate as the trees weaken. The original management decisions to plant short-lived trees, limit thinning and not create canopy openings that would allow more natural regeneration all contribute to the decline in forest health. Ornamental landscape plantings are overgrown and need revitalization. In addition, years of human use and the introduction of plants from other parts of the world threaten the fragile native habitats that once thrived here. Extensive management is imperative to keep them sustainable for preserving the scenic beauty and park setting of the Point Reyes and GGNRA as well as maintaining its historic character. Such management actions emphasize 1) variations in population densities and composition of forestry,

2) detection of invasive nonnative vegetation, 3) favorable habitat conditions that encourage regeneration, such as grass cover and small openings. All these require detailed and accurate mapping of vegetation in the parks and monitoring their change over time. Vegetation maps and associated information will also support a wide variety of other resource assessment, management, and conversation tasks (Ravan and Roy 1997; Ramsey and Nelson, 2002).

We mapped northern and southern park area separately with the specific training database. The northern area is covered by 26 frames of Digital Airborne Imagery System (DAIS) images (Fig 1) and the southern area is covered by 22 images (Fig 2). DAIS images at 1 meter

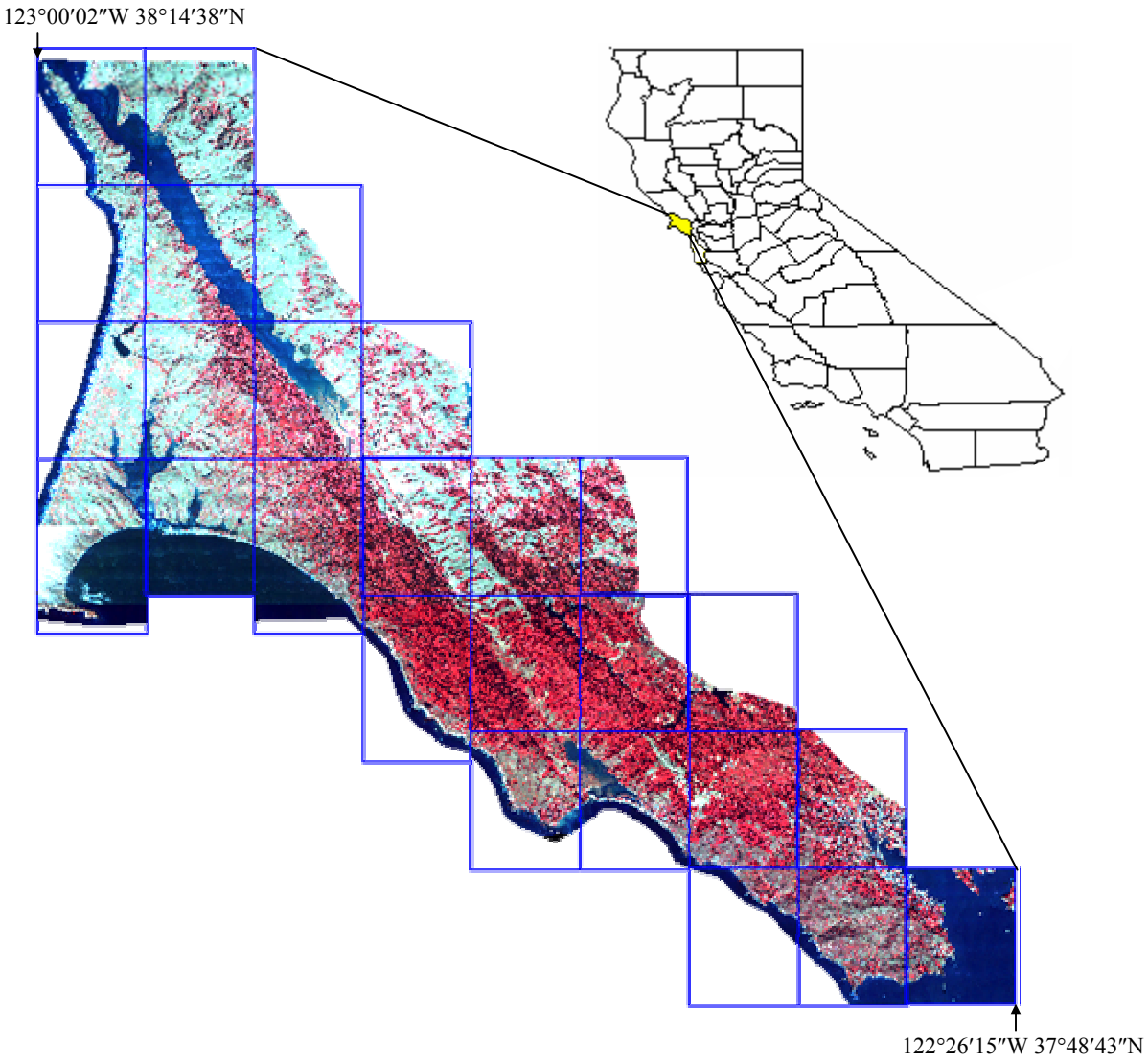

Figure 1. The nortern part of study site, rectangles show the boundary of image scenes.

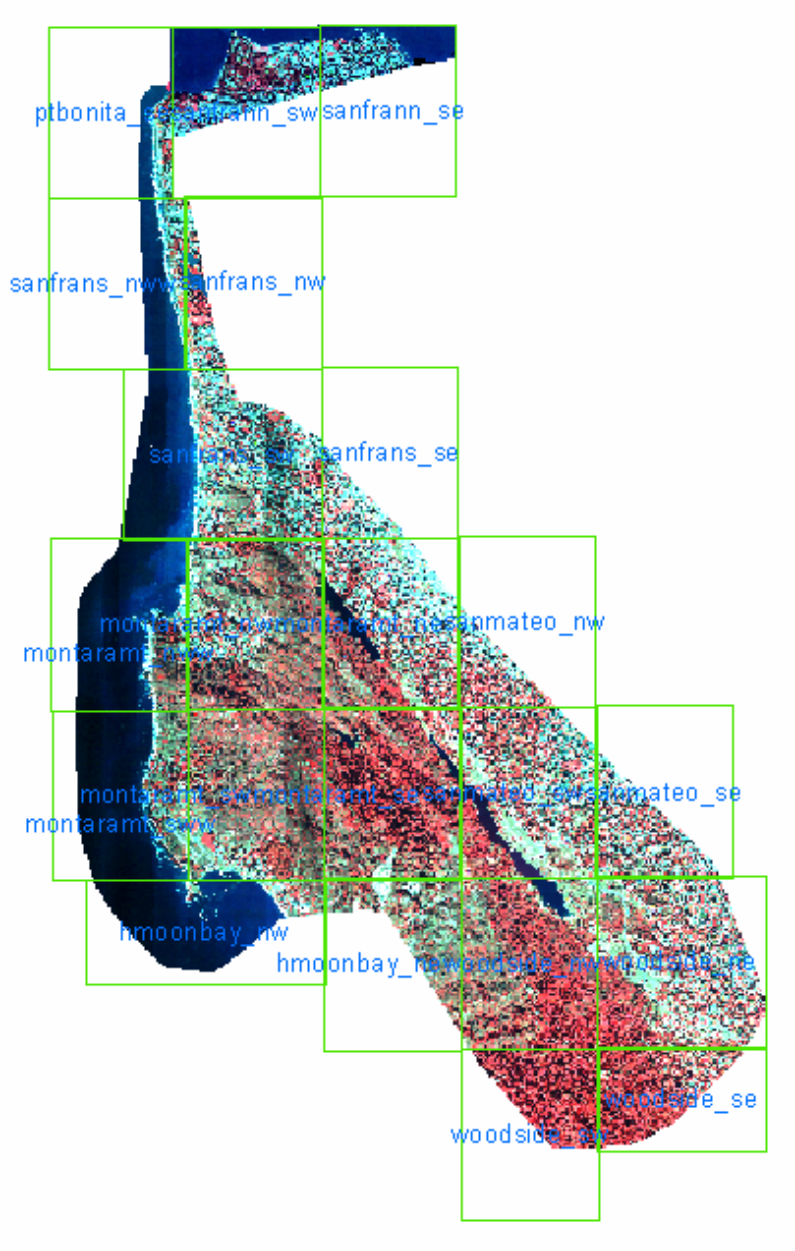

Figure 2. The nortern part of study site, rectangles show the boundary of image scenes.

spatial resolution were collected by Space Imaging at approximately 12:00-3:00 PM on Oct. 12-18, 2001. The images are composed of 4 bands: Blue (0.45-0.53μm), Green (0.52-0.61μm), Red (0.64-0.72μm), and Near-Infrared (0.77-0.88μm). DAIS is a 12-bit multispectral imaging sensor system for the generation of orthomosaics at ground sample distance ranging from 0.3 to 2 meters (Lutes, 2002). DAIS-1 began commercial operation in 1999 with the aim of complementing image products offered by space imaging's IKONOS satellite. The core of the system is a custom-built four-camera assembly utilizing narrow field-of-view sensors, with exterior orientation parameters provided by an onboard GPS/IMU navigation platform. GPS and inertial measurement unit (IMU) measurements are used to determine camera position and attitude for each image frame, instead of computing these parameters from ground control and tie points, so it is a direct georeferencing (DG) system. Tonal balance was conducted through all the images by the image provider, which removes the effect of uneven illumination of the image frames and guarantees the spectral consistency of each class among the multiple image frames. We also examined the consistency by F-test of some selected classes on selected image frames. The result indicates no significant difference in the spectral value for a certain class between any two selected images.

In addition to the 4-band DAIS images, we also included ancillary data for the classification. In many cases, image band derivatives and ancillary data sources can provide useful information to help distinguish between spectrally inseparable vegetation classes and lead to more effective vegetation classification. Environmental factors, such as elevation, slope, and soil moisture, are widely used ancillary data (Gould, 2000; Dymond and Johnson, 2002; McIver and Friedl, 2002). According to the habitat characteristics of vegetation, some environmental conditions are limiting factors to the spatial distribution of some species. For example, some species of willow (Salix), are predominantly located in riparian systems defined by close proximity to a watercourse or topographic depressions. For this reason, we incorporated topographic parameters including elevation, slope, aspect and distance to watercourses as additional features. We used a10-meter resolution DEM provided by the USGS (United States Geologic Service). Slope and aspect were two derivatives of the DEM. Distance to watercourses was calculated from a GIS vector file of watercourses provided by National Park Service. All the ancillary data were re-sampled to 1 meter to match the image pixel size.

For multispectral and hyperspectral image data, band ratio and spectral derivatives can also be used to improve classification accuracy of vegetation (Qi, 1996; Gould, 2000). Shadow in association with terrain effects is one of the significant barriers to vegetation classification with airborne high resolution multi-spectral images. The modulation of insolation due to crown shadow and terrain topography will lead to significant differences of intra-class spectral value and this modulation cannot be linearly modeled. Based on hue theory, hue is dependent on the spectral range and independent of illumination (Qi, 1996). We conducted an IHS transform and included intensity, hue and saturation as additional data layers in the classification to separate the effect of illumination to the quantity of intensity.

The classification scheme was designed at the alliance level according to the vegetation classification system of the California National Plant Society (CNPS) (The Vegetation Classification and Mapping Program, Sept. 2003 Edition), which is the sixth level in the seven-level hierarchy of the International Classification of Ecological Communities. At the alliance level, vegetation is classified based on dominant/diagnostic species, usually of the uppermost or dominant stratum. This level is more detailed than level 3 in the USGS land use and land cover classification system (Anderson et al., 1976). According to the PRNS survey database, this area is comprised of about 60 mapping alliances of forest, shrub and herb dominated ecosystems. We combined several alliances with very similar dominant species into the same classes and added several non-vegetation classes. Finally, we obtained 48 representative classes, in which 43 classes are vegetation alliances.

For northern area, our field samples were acquired from four sources: (1) the field survey plots (0.5 ha) from ground validation of a previous aerial photograph interpretation; (2) GPS acquisition of polygon features enclosing a field alliance or GPS acquisition of point features adjacent to a field alliance combined with image interpretation for inaccessible areas; (3) visual image interpretation aided by field reconnaissance; (4) for southern area, GIS data mapped Monterey Pine in 1998 using both hand drawn maps and some GPS, from Craig Scott (craig_scott@nps.gov). The survey database provides the UTM coordinates of the geometric centers of the field plots. However, the field survey plots were subjectively oriented and approximately sized, instead of fixed dimension or orientation. We created a 40-meter "plot" circle around each point and took those circular polygons as training regions, with area of approximately 0.5 hectare. This step constituted an approximation to the actual plot measurement.

The field survey described the sample plots to alliance level according to a vegetation key created specifically for the study site (Keeler-Wolf, 1999). It is worth noting that, according to the rules established in the classification protocol, the alliance designated for a particular plot need not contain a majority (by area) of the dominant species. It is possible that co-dominants are in equal representation to the species for which the alliance is named (for example, in the California Bay alliance, Coast live oak may have "up to 60% relative cover"). The GPS and field reconnaissance were intended to augment samples for the alliances with less than 10 plots to supplement our existing field survey plots database.

METHODS

1. Segmentation

In high spatial resolution imagery, a group of pixels can represent the characteristics of land cover targets better than single pixels, so we organize groups of adjacent pixels into objects and treat each of the objects as a minimum classification unit. Hay et al (2001) defined the objects as basic entities located within an image, where each pixel group is composed of similar digital values, and possesses an intrinsic size, shape, and geographic relationship with the real-world scene component it models. Therefore, the objects are spectrally more homogeneous within individual regions than between them and their neighbors. Ideally, they have distinct boundaries and they are compact and representative. According to these criteria, there are many means to identify objects, which are usually created by image segmentation. Segmentation here is a low-level processing, however, a very important foundation for subsequent classification because all object features are dependent on the objects derived through this process. Segmentation techniques in image processing can be categorized into global behavior based and local behavior based methods (Kartikeyan *et al.*, 1998). Global behavior-based methods group the pixels based on the analysis of the data in the feature space. Typical examples are clustering and histogram thresholding. Local behavior-based methods analyze the variation of spectral features in a small neighborhood. There are two important categories, edge detection and region extraction (Fu and Mui, 1981). Edge based methods locate the boundaries of an object according to the neighborhood spectral variation with edge detection algorithms, usually high-pass convolution algorithms such as differentiation. Region extraction can be further broken down into region growing, region dividing and hybrid methods, the first two of which are bottom up and top down algorithms, respectively. Region dividing/splitting iteratively breaks the image into a set of disjoint regions, which are internally coherent. Region merging/growing algorithms take some pixels as seeds and grow the regions around them based on certain homogeneity criteria.

However, not all of the segmentation techniques are feasible for the handling of high spatial resolution imagery. Global behavior based methods assume that an object forms a cluster in the feature space, i.e., similarity in spectral value (Kartikeyan *et al.*, 1998), which is often not the case for high resolution images. The high local variation often results in over-segmenting the regions within a small spatial extent. The regions obtained by this procedure are contiguous only

in the feature space, but not in the spatial domain. Edge based segmentation has not been very successful because of its poor performance in the detection of textured objects. On the other hand, small gaps between discontinuous edges allow merging of dissimilar regions (Kermad and Chehdi, 2002). In addition, edge detection from a multi-spectral image is complicated by the inconsistent location of edges in the multiple bands. A large number of image segmentation algorithms are based on region growing methods. This approach always provides closed boundary of objects and makes use of relatively large neighborhoods for decision making. Region growing requires consideration of seed selection, growing criteria, and processing order (Beaulieu and Goldberg, 1989; Gambotto, 1993; Adams and Bischof, 1994; Lemoigne and Tilton, 1995; Mehnert and Jackway, 1997). Some studies develop hybrid methods, in which edge or gradient information has been used in combination with region growing for image segmentation (Gambotto, 1993; Lemoigne and Tilton, 1995).

Although segmentation techniques are not new in the area of computer vision, they have been applied to classify remote sensing data only quite recently. The requirement of analyzing high resolution imagery and availability of commercial or non-commercial software packages catalysed a boost of their application (Blaschke et al., 2004). The ECHO algorithm is implemented in a free program called MultiSpec. It is a two-stage conjunctive object-seeking segmentation algorithm using statistical testing followed by a maximum likelihood object classification (Kettig and Landgrebe, 1976; Landgrebe, 1980). The more widely known commercial software for object-based image analysis is eCognition. The segmentation is conducted by the Fractal Net Evolution Approach (FNEA). FNEA is a bottom up region growing technique based on local criteria and starts with 1-pixel image objects. Image objects are pairwise merged one by one to form bigger objects. The merging criterion is that the average heterogeneity of image objects weighted by their sizes in pixels should be minimized (Baatz and Schape, 2000; Benz et al., 2004). Quantitatively, the definition of heterogeneity takes into account of both spectral variance and geometry of the objects. Figure 3 illustrates the segmentation results of the ISODATA algorithm (Iterative Self-Organizing Data Analysis Technique) and FNEA implemented in eCognition. ISODATA clustering is a typical global behavior based algorithm. It compares the spectral value of each pixel with predefined number of cluster centers and shifts the cluster mean values in a way that the majority of the pixels belongs to a cluster (Richards and Jia, 1999). The clustering process is optimized by merging, deleting

and splitting clusters. The objects segmented with the ISODATA algorithm are very small and dense at areas with a large gradient of spectral value, even though the number of cluster centers is set to be very small, for example, less than 10. This is a problem inherent to global behavior based algorithms since it only considers the difference in spectral space instead of spatial adjacency. FNEA minimizes average spectral heterogeneity/variance of pixels within an object and also considers spatial heterogeneity (Baatz and Schape, 2000; Baatz et al., 2001). This method can better delineate the boundaries of homogeneous patches and serve the pre-processing purpose of classification. We used eCognition segmentation in this project. We adopt this method because of its ability to take account of both spatial and spectral information in high resolution remote sensing imagery, its relative ease in realizing the processing of a large remote sensing dataset, its ability to include ancillary information in the segmentation process, and its fast execution. It is robust and has no parameters to tune and it is relatively easy to apply the output results in subsequent analysis.

The criterion of FNEA is that average heterogeneity of image objects weighted by their size in pixels should be minimized (Baatz and Schape, 2000). Quantitatively, the fusion value f is defined as

$$f = w \cdot \Delta h_{color} + (1-w) \cdot \Delta h_{shape}$$

where w is the user defined weight for spectral heterogeneity with $0 \le w \le 1$; Spectral heterogeneity h_{color} is defined as standard deviations (σ) of spectral value weighted by the object sizes (n); Δh_{color} is the difference of h_{color} after and before the merge:

$$\Delta h_{color} = \sum_c w_c (n_{merge} \cdot \sigma_c^{merge} - (n_{obj1} \cdot \sigma_c^{obj1} + n_{obj2} \cdot \sigma_c^{obj2}))$$

where w_c is the weight for each image channel. The shape criterion again is derived from compactness and smoothness.

$$\Delta h_{shape} = w_{cmpt} \cdot \Delta h_{cmpt} + (1-w_{cmpt}) \cdot \Delta h_{smooth}$$

where w_{cmpt} is the user defined weight for compactness with $0 \le w_{cmpt} \le 1$. h_{smooth} is defined as the ratio of the object perimeter to the perimeter of the bounding box, which depicts how similar the shape of an object is to a square; h_{cmpt} is defined as the ratio of the object perimeter to the square root of the object size, which characterizes how similar the shape of an object is to a circle. Both of them are weighted by the object size.

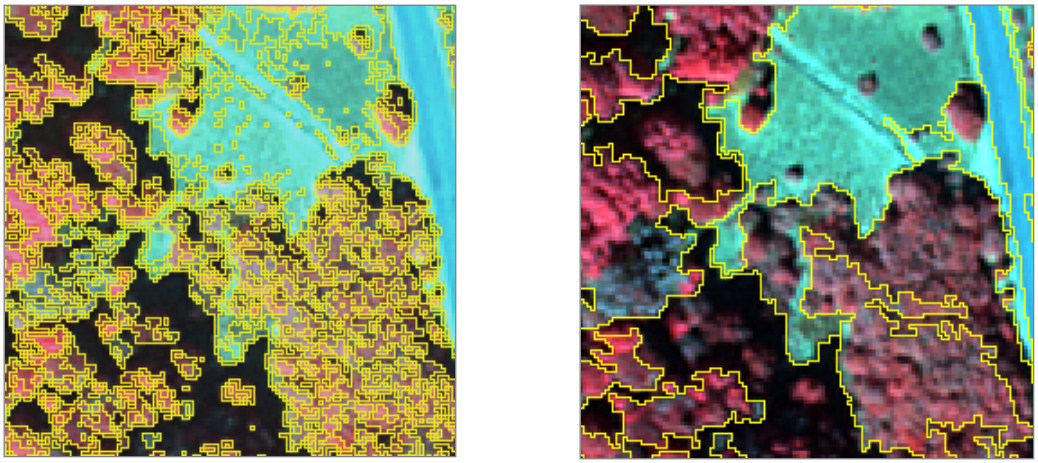

Figure 3 egmentation comparison (a) global based ISODATA method (8 clusters), (b) local region growing FNEA segmentation from eCognition.

2. Retrieval of land surface temperature (LST) from thermal images ETM+ 6

A large part of the southern area is covered by urban area. Since urban area usually appears to have higher temperature than vegetated area during the day time, we used 2 LST (Land Surface Temperature) of raining season (Mar 28, 2003) and dry season (Oct 3, 2002) as ancillary data for object-based classification, in addition to 4 topographical variables (elevation, slope, aspect and distance to water courses). We expect that the temperature could help to separate the urban area from very bright vegetated area, such as dry grass.

Based on the thermal radiance transfer equation, the Mono-Window Algorithm is adopted for retrieving LST from Landsat ETM+ band 6 data (Qin *et al.*, 2001). The procedure of LST retrieved from the ETM+ 6 thermal channel can be described in a flowchart (Fig 4). In the flowchart, input data are scaled thermal radiance (i.e., digital number). The MWA (Mono-Window Algorithm) needs three parameters: Atmospheric transmittance (t), land surface emissivity (e) and effective mean atmospheric temperature (Ta in K). Atmospheric transmittance is estimated from water vapor (Qin et al., 2001). Land surface emissivity depends on the land cover type. I classified the ETM images to three land cover types: water, vegetation and urban

and use specific emissivity for these 3 land cover types. Effective mean atmospheric temperature is the mean temperature at the satellite pass-by time of four meteorological stations in the study site (http://hurricane.ncdc.noaa.gov/CDO/cdo). After determining the three parameters and with input of ETM+6 Brightness Temperature, we can calculate the pixel-based LST with the MWA (Fig 5).

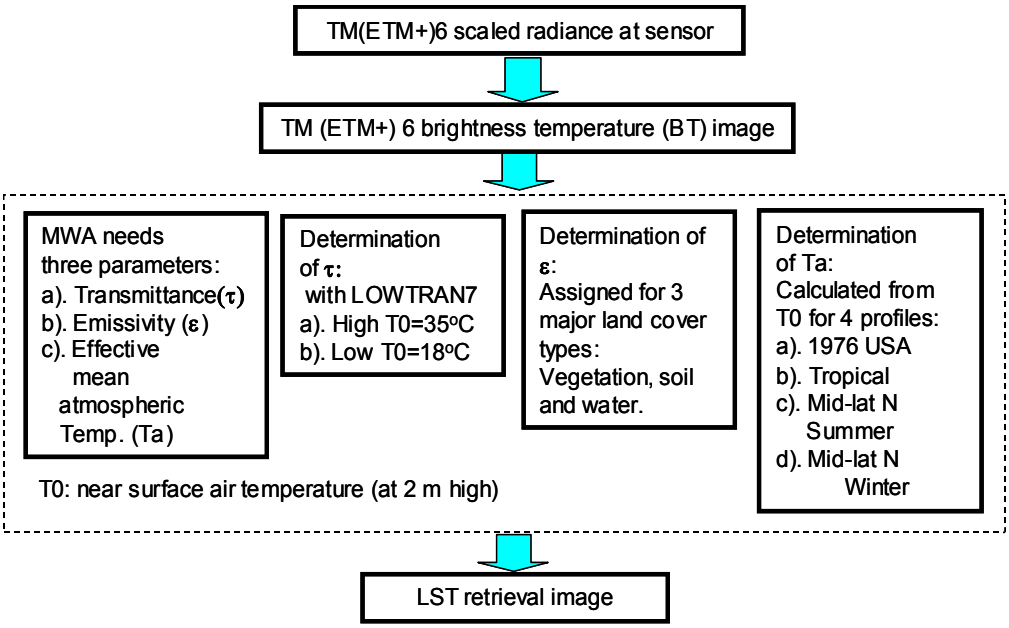

Figure 4 A flowchart of retrieving LST from the TM6 or ETM+6 thermal channel.

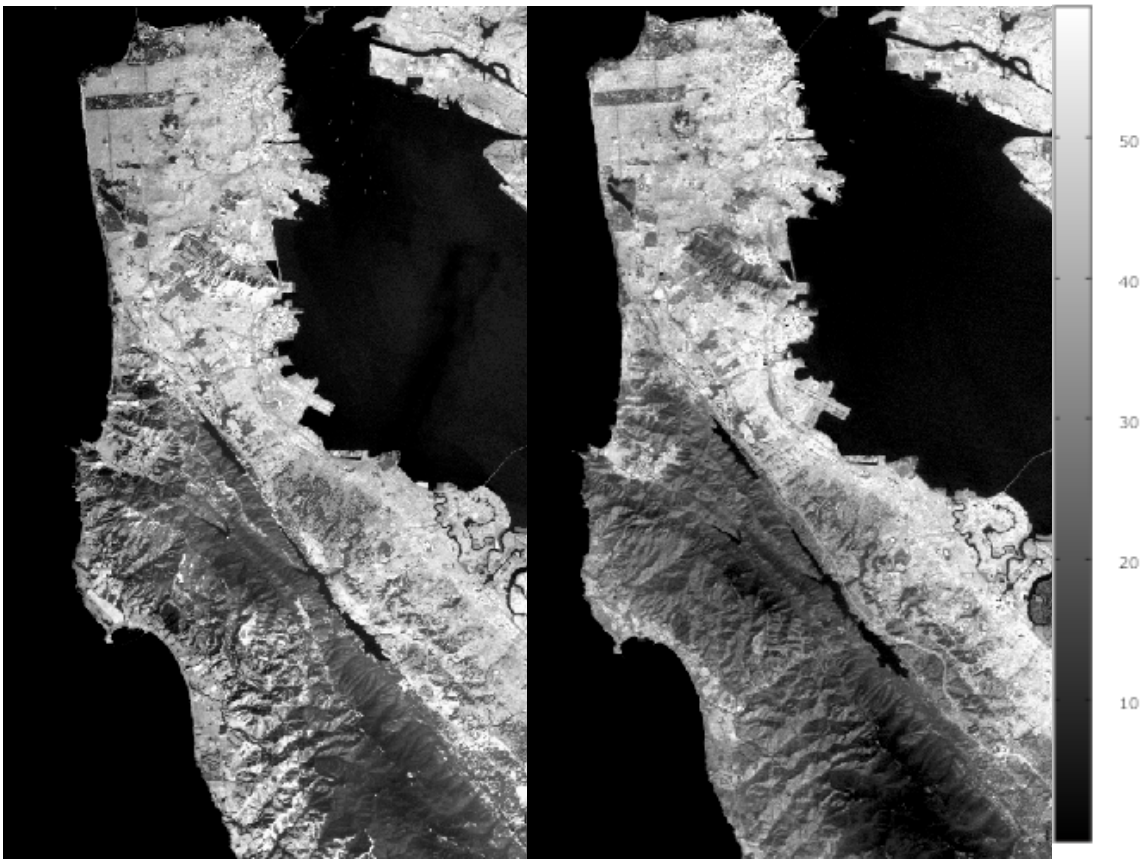

(a) (b)

Figure 5 Land Surface Temperature (^{o}C) a) Dry season, 10/3/2002; b) Raining season

3. Feature generation and selection

Features of each object, used in this analysis, were statistically derived from the 11 spectral and ancillary channels including 4 spectral bands, 3 IHS transform indices and 4 topographic parameters. We generated 52 features for each object in four categories (table 1): 1) 11 means and standard deviations respectively calculated from the band i values of all n pixels forming an image object (i=1,2, ..11), 2) 5 ratios calculated by band i mean value of an image object divided by the sum of all (band 1-4 and intensity) mean values (i=1,2,..5) of the 5 bands, 3) 16 shape features, 4) 9 GLCM (Grey Level Co-occurrence Matrix) and GLDV (Grey-Level Difference Vector) textures of the near infrared band. GLCM is a tabulation of how often different combinations of gray levels of two pixels at a fixed relative position occur in an image. A different co-occurrence matrix exists for each spatial relationship. GLDV is the sum of the diagonals of the GLCM. It counts the occurrence of references to the neighbor pixels' absolute

differences. Unlike pixel-based texture, GLCM and GLDV texture are calculated for all pixels of an image object, instead of for a regular window size. To reduce border effects, pixels bordering the image object directly (surrounding pixels with a distance of one) are additionally included in the calculation. In total, 52 features were calculated. All the features were linearly rescaled to the same range.

Based on the training object set, we employed the tree structured classifier CART to select a subset of features for classification in a stepwise manner. CART is a recursive and iterative procedure that partitions the feature space into smaller and smaller parts within which the class distribution becomes progressively more homogeneous (Breiman et al., 1984; Heikkonen and Varfis, 1998). The key of this iterative binary splitting process is to select one feature and its splitting value at a time to minimize node (equivalent to dataset) impurity. Node impurity reaches its minimum when the node contains training samples from only one class. This selection algorithm has a coincident mechanism in dividing the feature space with the following nearest neighbor classifier. A widely used impurity index, GINI is used in this study, which is named after its developer, the Italian statistician Corrado Gini (Breiman et al., 1984). Given a node t with estimated class probabilities $p(c \mid t)$, the measure of node impurity will be

$$i(t) = 1 - \sum_{c} p^2(c \mid t)$$

Each feature in the CART tree has an importance score based on how often and with what significance it serves as primary or surrogate splitter throughout the tree. The scores are quantified by the sum of the impurity decrease (ΔI) across all nodes that the feature has when it acts as a primary or surrogate splitter ($\tilde{s}_m$):

$$M(x_m) = \sum_{t \in T} \Delta I(\tilde{s}_m, t)$$

We selected the first 16 features according to the rank of the importance score for the classification.

Table 1 Object-based Features

Categories	Description	
Spectral features	Mean, Standard deviation and Ratio of DAIS bands 1-4, Intensity, Hue and Saturation	
	Brightness	Mean value of the mean of band 1-4 and intensity among pixels
Topographic features	Mean and Standard deviation of elevation, slope, aspect and distance to watercourses	
Textures	GLCM_Homogeneity	$\sum_{i,j=0}^{N-1} \frac{P_{i,j}}{1+(i-j)^2}$
	GLCM_Contrast	$\sum_{i,j=0}^{N-1} P_{i,j}(i-j)^2$
	GLCM_Dissimilarity	$\sum_{i,j=0}^{N-1} P_{i,j} \lvert i-j \rvert$
	GLCM_Entropy	$\sum_{i,j=0}^{N-1} P_{i,j}(-\ln P_{i,j})$
	GLCM_ Standard Deviation	$\sigma_{i,j}^2 - \sum_{i,j=0}^{N-1} P_{i,j}(i, j-\mu_{i,j})$ where $\mu_{i,j} = \sum_{i,j=0}^{N-1} P_{i,j} \Big/ N^2$
	GLCM_Correlation	$\sum_{i,j=0}^{N-1} P_{i,j} \left[\frac{(i-\mu_i)(j-\mu_j)}{\sqrt{(\sigma_i^2)(\sigma_j^2)}} \right]$
	GLDV_Angular Second Moment	$\sum_{k=0}^{N-1} V_k^2$
	GLDV_Entropy	$\sum_{k=0}^{N-1} V_k(-\ln V_k)$
	GLDV_Contrast	$\sum_{k=0}^{N-1} V_k k^2$
Geometric features	Area	True area covered by one pixel times the number of pixels forming the image object
	Length	Length of bounding box, approximately
	Width	Width of bounding box, approximately
	Compactness 1	The product of the length and the width of the corresponding Object and divided by the number of its inner pixels.
	Rectangular fit	Ratio of the area inside the fitting equiareal rectangle divided by the area of the object outside the rectangle.
	Border length	The sum of edges of the image object that are shared with other image objects.
	Shape index	The border length of the image object divided by four times the square root of its area. ie, smoothness.
	Density	The area covered by the image object divided by its radius
	Main direction	The direction of the major axis of the fitting ellipse.
	Asymmetry	The ratio of the lengths of minor and major axes of the fitting ellipse.
	Compactness 2	The ratio of the area of a polygon to the area of a circle with the same perimeter.
	Number of edges	The number of edges which form the polygon.
	Stddev of length of edges	The lengths of edges deviate from their mean value.
	Average length of edges	The average length of all of edges in a polygon.
	Length of longest edge	The length of the longest edge in a polygon.

* i is the row number and j is the column number, Vi,j is the value in the cell i,j of the matrix, Pi,j is the normalized value in the cell i,j , N is the number of rows or columns

4. Object-based classification

The parametric classification schemes such as the widely used MLC are not readily applicable to multi-source data and small object samples in this study because of their possible disparate nature (Srinivasan and Richards, 1990; Gong, 1996). K-nearest neighbor is a non-parametric classifier without any statistical assumption of the data distribution, which labels an unclassified object according to its nearest neighboring training object(s) in feature space. It is not widely used for pixel-based classification, partially due to its notoriously slow speed of execution (Hardin and Thomson, 1992). Unlike MLC, where training data are statistically condensed into covariance matrices and mean vectors, the K-NN classifier requires that the actual training vectors participate in each classification. However, for the object-based approach used in this study, the segments are minimum classification units, ie, classification primitives, instead of individual pixels. The amount of classification primitives is greatly reduced through the segmentation process. Therefore, the execution speed is not problematic. In this study, we test the K-NN for object-based classification while the conventional MLC was used in a pixel-based fashion as a benchmark.

To classify an object, K-NN finds the k neighbors nearest to the new sample from the training space based on a suitable similarity or distance metric. The plurality class among the nearest neighbors is the class label of the new sample. We measured similarity by the Euclidian distance in feature space. However, all class assignments in eCognition are determined by assignment values in the range 0 (no assignment) to 1 (full assignment). The closer an image object is located in the feature space to a sample of class A, the higher the membership degree to this class. eCognition computes the distance as follows:

$$d = \sqrt{\sum_f \left(\frac{v_f^{(s)} - v_f^{(0)}}{\sigma_f} \right)^2}$$

d - Distance between sample object s and image object o.

$v_f^{(s)}$ - Feature value of sample object for feature f.

$v_f^{(0)}$ - Feature value of image object for feature f.

σ_f - Standard deviation of the feature values for feature f.

The distance in the feature space between a sample object and the image object to be classified is standardized by the standard deviation of all feature values. Thus, features of varying range can be combined in the feature space for classification. Due to the standardization, a distance value of d = 1 means that the distance equals the standard deviation of all feature values of the features defining the feature space. Based on the distance d a multidimensional, exponential membership function z(d) is computed as

$$z(d) = e^{-k \cdot d^2}$$

The parameter k determines the decrease of z(d), which can be defined with the variable function slope.

$$k = ln(1 / function\ slope)$$

The variable function slope equals z(d=1) (fig. 6a). Thus, the function slope is the membership value of an image object to a class, if the closest sample object of that class has a distance to the image object which equals the standard deviation of the feature values from the closest sample object. In this project, we use the function slope with the value of 0.2.

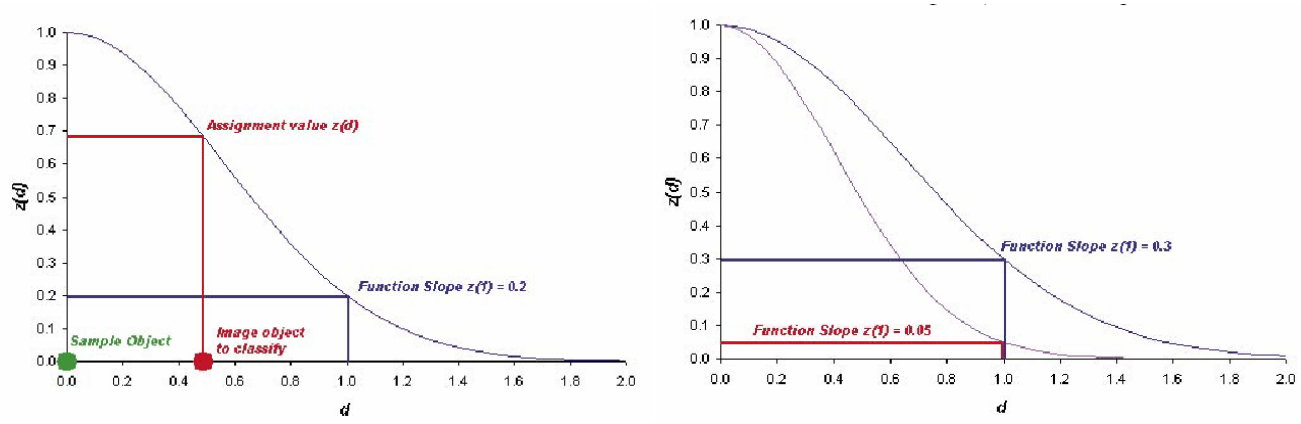

(a) (b)

Fig 6. Nearest neighbor membership function (a) a membership function is computed depending on the function slope; (b) different membership values for the same object for different function slopes.

In this project, the leave-one-out method was used to assess K-NN classification accuracy. Specifically, we took one sample object out of the training sample set and used it as a (singleton) test set and all others as training. This was repeated until all the observations had been used as

singleton test sets. When all observations have been left out once, i.e., classified once, the results are pooled and the classification accuracy is calculated (Steele et al., 1998).

Although our final classification objective is at the alliance level, we first classified all objects into four wider categories: forest, shrub, herbaceous and others, and then further classified each category to a more detailed alliance level. We designed this two-level hierarchical classification because it is relatively easy to classify the entire project area into those four types and we assumed that each of the four categories had different favorable feature subsets to be used for classification. Parallel classification of many classes is more likely to give poor classification accuracy (San Miguel-Ayanz and Biging, 1997). Therefore, once we separated the four categories, we conducted feature selection for each of them. Generally speaking, the four broad categories are very different in spectral space and easy to classify.

In the K nearest neighbor (K-NN) algorithm, K is a parameter representing how many samples are considered in classifying one object with unknown type. A smaller k needs less processing time, but may not achieve the best classification accuracy. To test the sensitivity of classification accuracy to K, we varied K from 1 to 18 and classified all the training objects with the K-NN classifier, and then compared the overall and average accuracies. Different classes achieved the highest classification accuracy at different k values, which is illustrated in figure 7. One dot represents one class. The x-axis is the number of sample objects for this class in logarithmic scale. The y-axis is the K that gives the highest accuracy to this class, referred as best K. It is obvious that larger K values tend to favor classes with larger sample sizes. However, if we use the median of the best K for each broad category, the average and overall accuracies were 47.5% and 56.8%, respectively, which are not significantly different compared with 50.9% and 56.3% using first nearest neighbor (k=1). The median of the best K in the four categories forest, shrub, herb and non-vegetation were 4, 3, 2 and 3, respectively. Since the classification accuracies of many classes with small sample size are reduced, the average accuracy is actually lowered in classification with median K. The above analysis shows that using a median K as the tradeoff in this classification will not benefit the entire classification. Therefore, we simply used 1-NN in the following object-based classification.

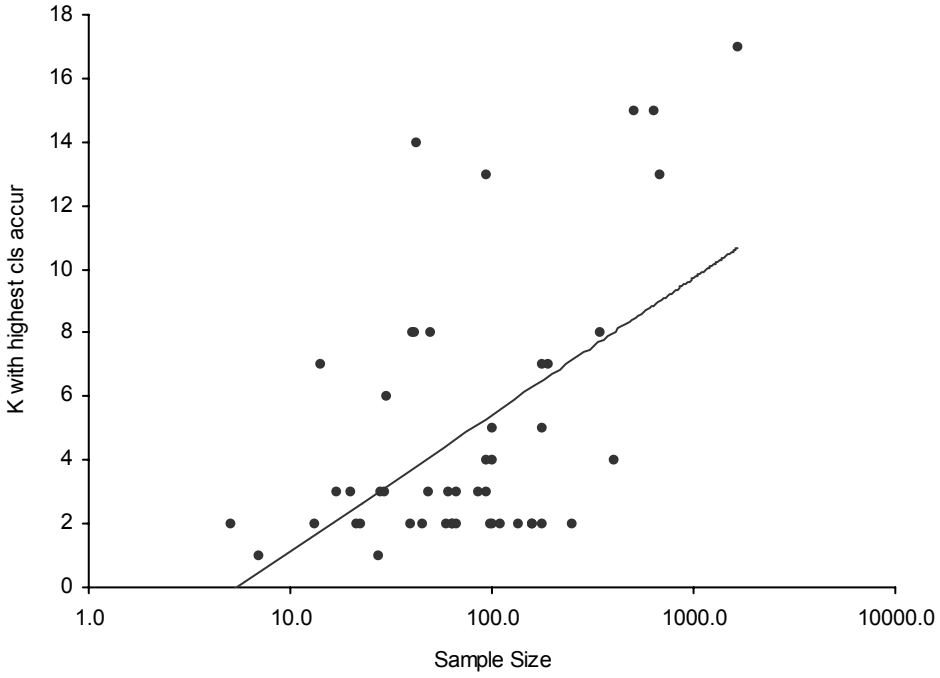

Figure 7. Best K for each class with respect to sample size in number of pixels

For comparison, we used the same training set to perform the pixel-based MLC which has generally been proven to be one of the most robust classifiers for remote sensing data (San Miguel-Ayanz and Biging, 1996). The pixel-based MLC is a good benchmark to evaluate the performance of the object-based K-NN. The same feature sets were used except that we removed the features specific to objects, such as geometric features and standard deviations (Table 2). For pixel-based MLC, we calculated all the features and conducted the classification in PCI v9.1 (PCI Geomatics Enterprises Inc.). The texture features were derived with a window size of 25×25 (Hodgson, 1998). Since the whole study site is composed of 26 images, the dataset is too large to handle if all the images are merged. Alternatively, we only conducted classification on training samples to serve this comparison purpose. After computing all the classification features for each pixel in all images, we merged all the training pixels from the 26 frames to one frame without keeping the spatial relationship. Each feature was stored in one channel. Then, we classified this merged image. We did not separate the training and test samples because we wanted to keep the equivalent sample size to the leave-one-out method in 1-NN. Otherwise, this comparison will favor 1-NN.

Table 2 Rank of features selected for 1-NN and MLC from CART

Features for each object		Object-based 1-NN				Pixel-based MLC			
		Forest	Shrub	Herb	Others	Forest	Shrub	Herb	Others
DAIS band 1	Mean	7	1			7	2		
	Standard Deviation	10				---			
DAIS band 2	Mean		7	12			7	8	
	Standard Deviation	11				---			
	Ratio	6	6			6	6		
DAIS band 3	Mean		16				14		
	Standard Deviation				11	---			
	Ratio	5				5			
DAIS band 4	Mean		14	11	16		13	7	12
	Standard Deviation		15		3	---			
	Ratio	8	8		13	8	8		9
	GLCM Homogeneity				10				7
	GLCM Contrast		12	8	6		11	4	5
	GLCM Dissimilarity	15	11		12	11	10		8
	GLCM Entropy				9				6
	GLCM Standard Deviation		13		15		12		11
	GLCM Correlation	9				9			
	GLDV Angular Second Moment				14				10
	GLDV Entropy			15				11	
	GLDV Contrast			14	5			10	4
IHS- Intensity	Mean			13				9	
	Ratio	16				12			
IHS- Hue	Mean	13				10			
IHS- Saturation	Mean	4	5			4	5		
Elevation	Mean	1	1	1	2	1	1	1	2
	Standard Deviation	12		6	7	---			
Slope	Mean	3	4	3		3	4	2	
	Standard Deviation	14	10	4	8	---			
Aspect	Mean		9	5	4		9	3	3
	Standard Deviation			7		---			
Dist. to watercorses	Mean	2	3	2	1	2	3	2	1
Brightness				9				5	
Stddev of length of edges				10					

RESULTS AND DISCUSSION

1. Object generation

Based on the 4-band DAIS imagery and the intensity layer, we segmented the images into homogeneous objects with eCognition 4.0. We adjusted the segmentation scale parameters to best delineate small homogenous vegetation patches, approximately in the size of several canopies. The final criteria of segmentation consisted of spectral homogeneity and geometric indices with the weights of 0.7 and 0.3, respectively. The two geometric indices, compactness and smoothness, were assigned equal weight. The size of the objects depended on the variation of the spectral values over spatial neighbors. The objects were larger in areas with mostly herbaceous cover, and smaller in forested areas because of the different spatial variation in spectral values between these classes. This adaptive segmentation may significantly reduce the quantity of the data for further processing and classification while still conserving spectral variation information. Any image object overlapping with the training regions by more than 10% of its own area was treated as a training object. This percentage was determined based on our visual interpretation of the ratio of intersected area to the area of major image objects. Larger percentages will generate less training objects and small percentages can not guarantee that the training objects are dominated by the same species as the one represented by the training region. Figure 8 illustrates the result of eCognition segmentation and training object generation in a small part of our study site.

From the above procedure, 6,923 training objects were identified. After categorizing those training objects into 48 classes, we found the sample sizes were extremely uneven by class (Table. 2). The coyote brush had the largest sample size of 1,158 training objects while the coast buckwheat had only five training objects. This situation is normal for vegetation classification since the size of training samples is proportional to the abundance of vegetation on the landscape. For a rarely distributed species, it is difficult to collect more samples. In consideration of this, we chose nonparametric methods both for feature selection and classification.

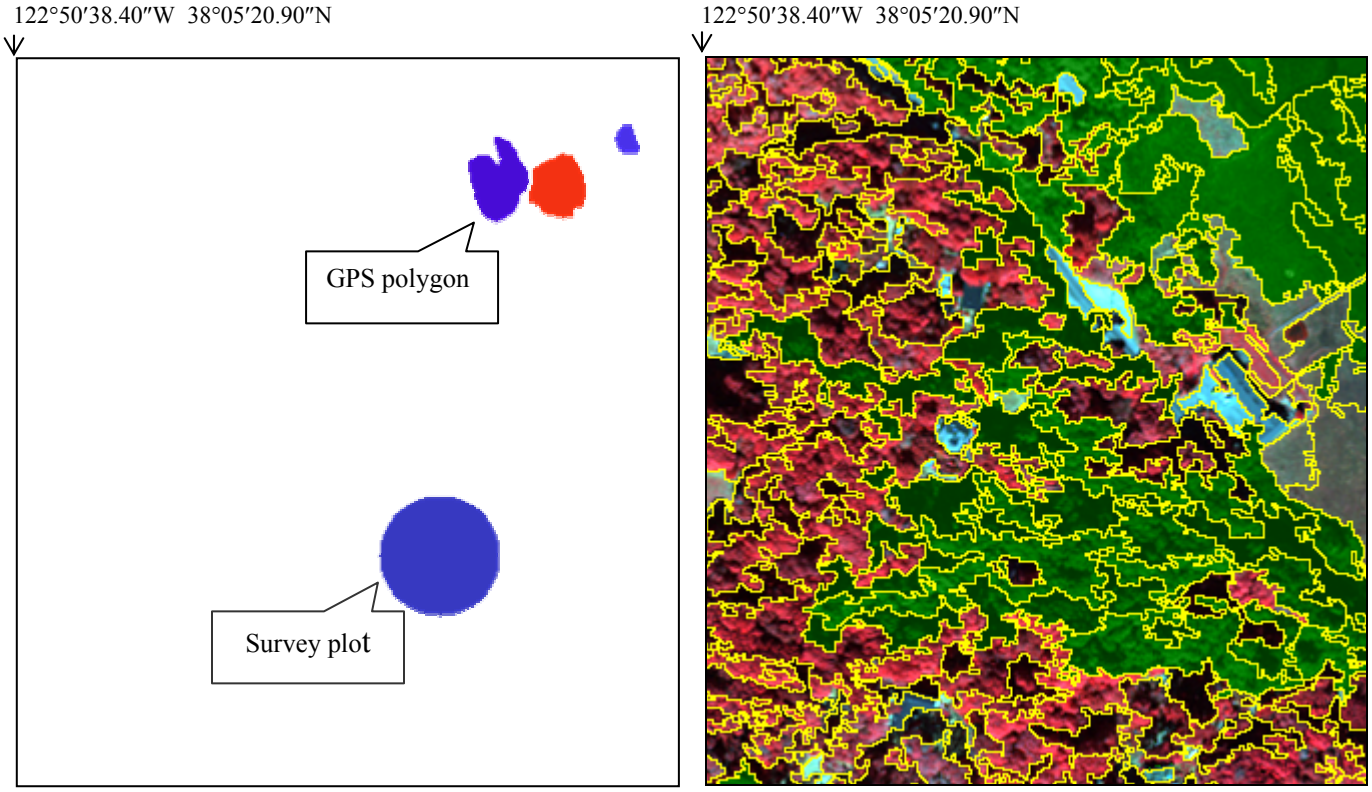

(a) (b)

Figure 8. Training sample selection: (a) a small part of training regions, 4 polygons for 2 classes (blue and red respectively), (b) intersected polygons as training objects in green overlaid on original image

2. Feature selection

The purpose of feature selection is to reduce the computational requirements while preserving the overall accuracy of classification. The 52 features for each object were ranked by a CART process. Using CART, we generated 11 feature sets with different numbers of features: the first 2, 7, 12, 17 and so on until all 52 features were reached with an interval of 5, according to the feature importance ranking. Using each of the resultant feature sets, we conducted classifications by programming in Matlab and compared their classification accuracies. In the 1-NN classification, both average and overall accuracies increase with the inclusion of more features at the beginning, then drop when we include more than 12-17 and 22-27 features,

respectively (Fig. 9). To achieve higher average accuracy, we selected the first 16 features out of the 52 features for further classification.

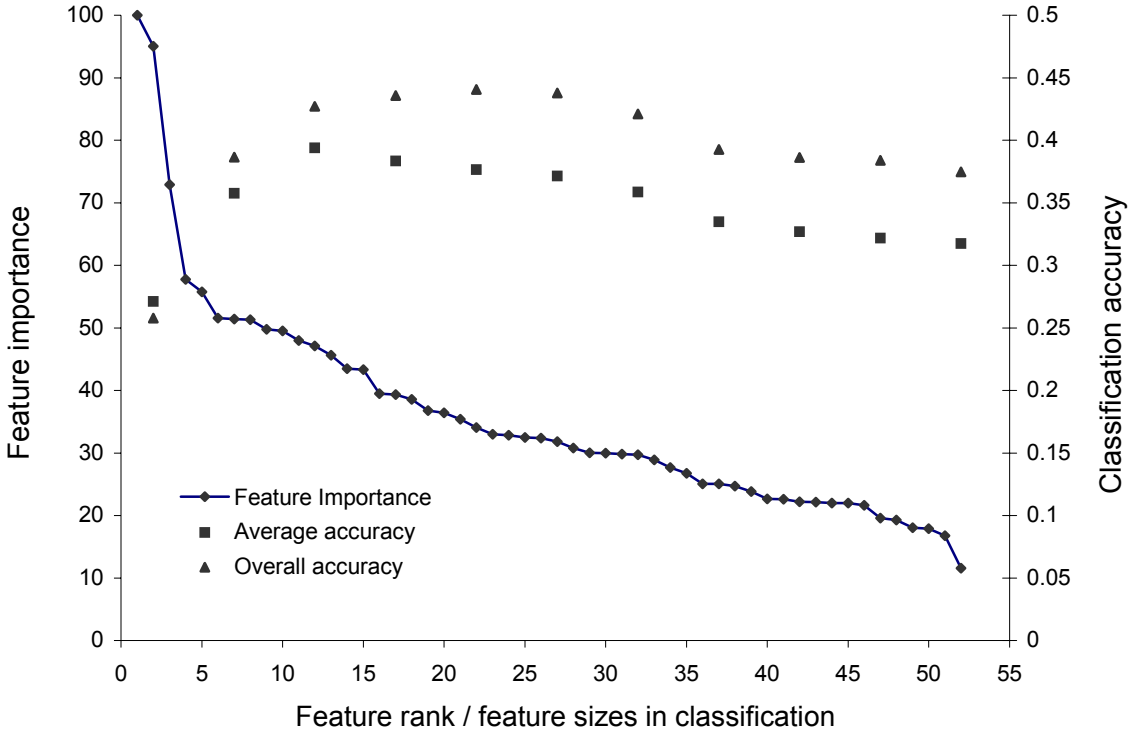

Figure 9. Rank of feature importance assessed by CART and classification accuracy vs. number of features used

In the process of choosing the number of features for classification, we found only 38.9% average accuracy and 44.2% overall accuracy could be obtained when classifying 48 classes at the same time. Among the 43 vegetation alliances, 26 alliances were frequently confused with the relatively abundant rush and coyote brush. Those two alliances have large sample sizes and extend sparsely in feature space because of large spectral variation in such large geographical extent of the whole study site. Classification accuracies of the alliances with small sample sizes were highly affected by these alliances. Feasibly in each frame, we could separate the top four categories of forest, shrub, herb and non-vegetation with 1-NN rule based on the 6 features of bands 1-4, NDVI and Hue with higher than 95% accuracy. The features of the alliances with a

larger sample size were not so dispersed or dominant in feature space for each frame. For each category, we selected the best feature sets for classification. Table 4 lists the numbers of features selected among spectral features, topographic features, textures and geometric features for each category. Among the top 16 features, there are 5-7 high-ranking topographic features and three textures. Elevation, distance to watercourses, slope and aspect are the features most capable to separate the vegetation alliances. Vegetation species distribution appeared to be associated with topographic features. This can be explained by the fact that naturally growing species are adaptive to environmental factors, such as humidity and sunlight, which are related to topography. For forest, shrub and herb, topographic features become more and more important, while spectral features are less essential. This is reasonable since forest is more resistant and less dependent on environmental conditions compared with shrub and herb in terms of plant biology (Barbour et al., 1999). The images were acquired during the dry season in California. Except for riparian vegetation, most herbaceous plants are dehydrated and/or dead. For this reason, spectral differences can hardly separate the herb alliances.

Table 3 Types of features selected for classification

	Spectral feature(20)*			Texture(9)	Topography(8)		Geometry(15)
	Mean(8)	Std.dev(7)	Ratio(5)		Mean(4)	Std.dev(4)	
Forest	3	2	4	2	3	2	0
Shrub	5	1	2	3	4	1	0
Herb	4	1	0	3	4	3	1
Non-veg	1	2	1	7	3	2	0

* the number of features in this category selected from 52 features.

Two or three out of the nine texture features, such as contrast, correlation and dissimilarity are important features in the classification, which can represent the appearance of vegetation. This is not a very large percentage because the features were selected within each category. The textures of the four upper level vegetation categories are more distinct from each other than the textures of alliances within the categories. For example, the crown structures of different forest alliances are irregular and not easy to capture by texture, while the textural differences between forests and shrubs are fairly easy to detect.

Unlike in the classification of human-made features, geometric features did not significantly contribute to the classification of vegetation at this level of image resolution, although they are features unique to the object-based approach. Tree crown spectral values are

highly variable due to textures, shadows and gaps present in high resolution airborne images. Therefore, the shape of the objects has no obvious pattern that could be used as evidence for classification. Only the standard deviation of length of edges ranked high (10th) in herb classification. Compared with forest, herb objects are more compact and the edges are more smooth and regular. Therefore, the geometric properties of herb dominated image objects are relatively unique.

For the southern area, we included 16 features in the classification: 1-4 DAIS band, elevation, slope, aspect, distance to water courses, intensity, hue, saturation, 2 LST and three textures. According to Clausi (2002), a preferable choice of texture statistics is the combined use of the fairly independent statistics: contrast, entropy and correlation. So these three textures were included as classification features. For all of the 22 images, we calculated the 16 features for each sample object and saved the sample features as a classification sample base. Then, each image was classified respectively according to this sample base.

3. Object-based classification

At the first, we performed the classification for training/test samples in Matlab for its coding advantage. It is flexible for us to select classification features, examine classification parameter K and test classification accuracy with the pooled samples from all images. The segmented objects from eCognition were exported in vector format with features in an attribute table. The object based classification was conducted with these attribute features. After we got the knowledge about the significant features, we implemented the classification for each image in eCognition. Each broad category had a specific set of 16 features selected from all features for classification, although there were many overlaps. Table 4 shows the classification accuracy for each class. The accuracies for vegetation classes varied greatly. The average and overall accuracy were 50.9 % and 56.3%, respectively. Among 43 vegetation classes, 14 classes had an accuracy higher than 60%. Besides the objective similarity of spectral characteristics, explanations for the lower accuracy among some classes are threefold: 1) they have small sample sizes, such as gorse and cordgrass; 2) they are understory vegetation, such as mixed manzanita and poison oak; and 3) the alliance itself is composed of a dominate species associated with another species ecologically, such as California Bay and Coast live oak.

These results suggest that there is a criterion discrepancy between image classification and the botanical mapping. In the project, some sample plots are covered by vegetation associations instead of homogeneous species. For example, Douglas-fir, California Bay and Coast live oak are common ecological associates. A training object that is claimed as 'Douglas-fir' may contain as little as 15% Douglas-fir by canopy area, according to the field and photo classification protocol. This fact is reflected in the vegetation classification protocols developed for the project area (Keeler-Wolf, 1999). This problem was also addressed by Kalliola and Syrjanen (1991). Therefore, the spectral feature of the mixed object is intermediate according to the proportion

Table 4 Sample size and classification accuracy

Class	Sample size		Accuracy (%)		Class	Sample size		Accuracy (%)	
	Object	Pixel	NN	MLC		Object	Pixel	NN	MLC
California Bay	640	2514769	49.40	19.71	Hazel	17	97783	61.21	93.97
Eucalyptus	93	283175	61.79	70.65	Poison Oak	49	279488	16.13	51.94
Tanoak	27	146585	72.87	76.99	Salmonberry	63	252435	22.77	60.29
Giant Chinquapin	30	165041	25.80	63.01	Arroyo Willow	159	724783	38.12	32.92
Douglas fir	675	2938898	61.61	26.66	Pacific Reedgrass	176	1033935	56.77	62.94
Coast redwood	190	788839	60.90	65.92	European Dunegrass	63	208655	100.00	65.33
Bishop pine	398	2068280	68.68	55.36	Perennial Grasslands	248	1505509	48.88	32.24
Monterey cypress/pine	85	309727	39.91	55.67	Saltgrass	101	386005	61.64	28.32
Willow Mapping Unit	158	556823	41.10	44.74	Rush	508	2649631	32.89	24.89
Red Alder	339	1198298	37.03	12.20	Tufted Hairgrass	28	131875	58.61	86.11
Coast Live Oak	176	700902	42.17	18.76	Bulrush-cattail spikerush	59	306018	50.03	67.8
California Buckeye	22	61766	16.49	83.15	Cordgrass	14	108248	28.00	70.58
Yellow bush lupine	61	216909	42.71	73.36	Iceplant	100	328552	51.08	51.98
California Wax Myrtle	97	441703	30.05	54.84	Coast Buckwheat	5	52909	51.81	97.17
Blue blossom	133	789096	55.27	63.72	Dune sagebrush-goldenbush	67	276225	26.69	33.66
Chamise	66	280686	59.57	74.94	Pickleweed	177	920125	21.33	68.76
Eastwood Manzanita	42	172663	32.71	71.16	California annual grassland weedy	109	627317	69.96	39.75
Coffeeberry	40	162152	21.88	61.43	California annual grassland	93	469983	69.09	76.11
Mixed Manzanita	39	228206	41.75	64.01	Purple Needlegrass	7	22934	99.29	74.68
Sensitive manzanita	29	168417	61.46	60.45	Urban	94	150991	85.51	92.76
Mixed Broom	100	433219	70.63	75.43	Non-vegatated	13	16705	94.91	91.28
Coyote Brush	1158	7585795	78.06	27.37	Dune	21	53578	40.18	98.03
California Sagebrush	45	174285	34.30	83.22	Beaches	41	183635	63.29	94.76
Gorse	20	101433	4.14	75.11	Water	48	833694	90.82	92.90

of associate species. While significant percentages of the training objects were classified as discrepant alliances, it is very likely that these percentages represent the composition of vegetation in the training objects. This is due to the fact that the training objects were classified according to a set of rules that does not include homogeneity as a requirement for classification to a particular alliance. Thus, it is not unreasonable to assume that a fairly high accuracy has been obtained when the percentages of alliances "confused" with a reference alliance is within the tolerances specified by the original classification guidelines for the training data, and those "confused" alliances are common ecological associates with the reference alliance. For these reasons, traditional metrics of classification accuracy are misleading. Table 5 illustrates this phenomenon. The classification accuracy of Douglas-fir, California Bay and Coast live oak are only 61%, 62% and 51%, respectively, but 70%-90% of the objects are classified into their ecological associates. That means most confusion occurs in the ecological associates of these three species. This implies that if we group these classes in one higher level class in a hierarchical classification system, we would expect an better classification accuracy.

Table 5 Classification Confusion Matrix of California bay, Douglas-fir and Coast live oak

Class	California bay	Douglas-fir	Coast live oak
California Bay	329	111	20
Douglas fir	93	412	37
Coast live oak	23	22	118
Others	195	130	15
Sample size	640	675	190
Accuracy	51%	61%	62%
Classified into associates	70%	81%	92%

In order to compare with pixel-based MLC, the classifications result from the object-based approach was represented in raster format. The accuracy was then calculated based on the number of correctly classified pixels for each class. The average accuracy and overall accuracy of the object-based 1-NN were 51.03% and 58.37%, respectively (Fig. 10); they were 61.81% and 41.38% for the pixel-based MLC. The average accuracy of the MLC was nearly 10 percent

higher than that of the 1-NN, while the overall accuracy was 17 percent lower. This illustrates that the MLC has some advantage in classifying those classes with small sample sizes, such as gorse and cordgrass. Figure 11 a & b illustrate this relationship of classification accuracy with respect to sample size in number of objects and number of pixels, respectively. The accuracy of 1-NN for each class has no obvious pattern, while that of MLC decreases apparently when the sample size increases.

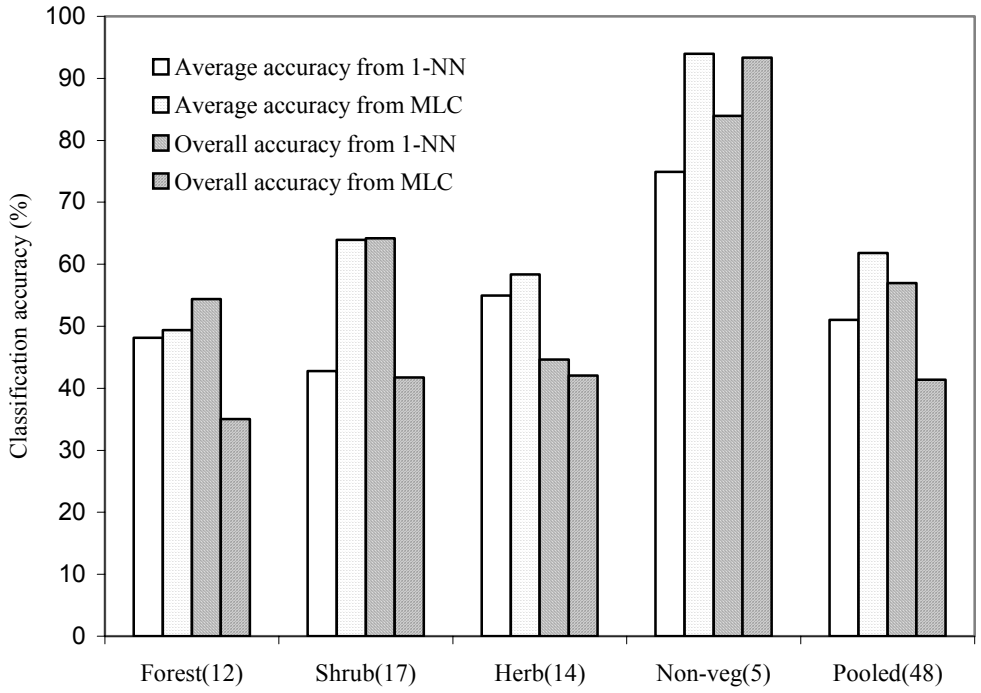

* the number in the bracket is the number of alliances/classes in this categories.

Figure 10. Comparison of classification accuracies generated by 1-NN and MLC

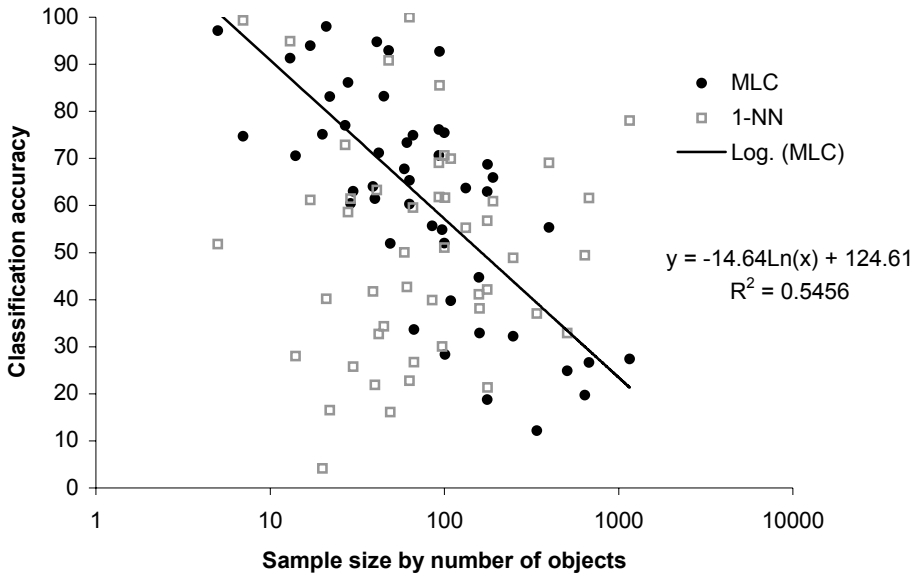

(a)

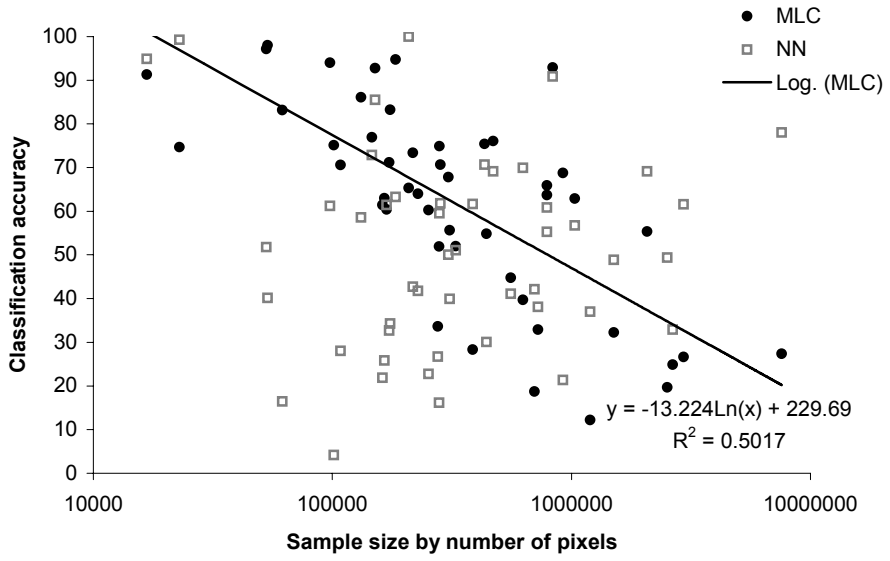

(b)

Figure 11. Classification accuracy for 48 classes with respect to (a) sample size in number of objects, (b) sample size in number of pixels

These results indicate that object-based 1-NN is more robust with respect to sample size. Vegetation classification is different from generic land cover classification. The alliance is more likely to be a botanical concept. The appearance of the same alliance on images always deviates from the typical representation caused by shadow, density, size, intermediate type and transition zones, which are difficult to be considered by computer-based remote sensing image classification. In addition, the training samples were not collected randomly to the practical constraints associated with validation efforts. Therefore, a larger sample size does not necessarily mean that the features are closer to a normal distribution. Whereas alliances with large samples always imply their extensive geographical distribution, variable physiognomy at the landscape level results in a lack of normality in feature space. Therefore, a pixel-based MLC cannot achieve an optimal solution with this non-unimodel data. Object-based 1-NN is a non-parametric method and it relaxes the restrictions of MLC. It is more flexible and adaptable to all data models as long as the training samples are representative of the whole dataset.

SUMMARY AND CONCLUSIONS

In this project, high resolution airborne remote sensing images from the DAIS sensor were employed to classify 43 vegetation alliances plus 5 non-vegetation classes over 180,000 acres in Point Reyes National Seashore, California, covered by 26 frames of images. To overcome the high local variation, we used an object-based approach and examined a set of suitable methods of feature extraction and classification. We performed image segmentation in eCognition (Baatz et al., 2001). In consideration of the uneven training sample sizes, we selected non-parametric methods for both feature selection and classification. We first separated the 48 alliances into forest, shrub, herb and non-vegetation and then conducted feature selection and classification within each category individually. The tree-based CART algorithm was used to select the most important features for classification. After testing the sensitivity of the classification accuracy to parameter k of the k-nearest neighbor classifier, we chose the first nearest neighbor to perform classification. Pixel-based MLC was used as a benchmark in evaluating our approach.

In this work we found that using objects as minimum classification units helped overcome the problem of salt-and-pepper effects resulting from traditional pixel-based classification methods. Among spectral, topographic, texture and geometric features of an object, topographic information as ancillary data were important for natural vegetation classification at this spatial scale of this project, especially for environment-dependent alliances. New geometric features did not significantly contribute to vegetation classification. The use of a hierarchical classification scheme helped improve the accuracy considerably, mainly because optimal features in classification were selected for each broad category. The object-based 1-NN method outperformed pixel-based MLC algorithm by 17 percent in overall accuracy. Meanwhile, pixel-based MLC achieved higher average accuracy because it performed better in the classification of alliances with small sample sizes. The results indicate that object-based 1-NN method is more robust than pixel-based MLC due to the specific characteristics of vegetation classification in our study area.

Although the average accuracy and overall accuracy are only approximately 51% and 58%, respectively, 13 alliances among the 43 vegetation alliances achieved the results with accuracy of 60% and higher. We report the accuracies with the assumption that broad groups (forest, shrub, herb and non-vegetation) are fully correctly classified. Additionally, we found that traditional

assessments of classification accuracy may not be suitable in heterogeneous systems. This is especially true when rules for on-the-ground vegetation classification are based on ecological relationships and when classification rules for remotely sensed imagery are statistically based. A revised set of procedures for reconciling ecological dominance with image classification is required for this purpose.

We found that the accuracy of detailed vegetation classification with very high resolution imagery is highly dependent on the sample size, sampling quality, classification scheme and structure and ground vegetation distribution. These data could be further refined in future vegetation classification efforts involving such a high level of thematic detail. A potential improvement to the method described by this paper may be to examine in more detail the automatic intersection of survey plots and objects. Some sample objects are not covered or dominated by a single alliance due to inherent landscape heterogeneity.

This work shows promise of the use of high spatial resolution remote sensing in detailed vegetation mapping. With the object-based classification, vegetation classification accuracy is significantly improved and substantially surpasses 40%, which has been considered as a barrier in remote sensing based mapping of complex vegetation.

ACKNOWLEDGEMENTS

This research was supported by the National Park Service. We are grateful to Dave Schirokauer and Pam Van Der Leeden for providing us with help in field sample collection and valuable suggestions in the work. Suggestions from Ruiliang Pu improved this work.

REFERENCES

Adams, R. and L. Bischof, 1994. Seeded region growing, *IEEE Transactions on Pattern Analysis and Machine Intelligence*, 16(6):641-647.

Anderson, J. R., E. E. Hardy, J. T. Roach and R. E. Witmer, 1976. *A Land use and land cover classification system for use with remote sensor data,* USGS Professional Paper #964, p.

Baatz, M., M. Heynen, P. Hofmann, I. Lingenfelder, M. Mimier, A. Schape, M. Weber and G. Willhauck, 2001. *eCognition User Guide 2.0: Object Oriented Image Analysis,* Definiens Imaging GmbH, Munich, Germany, 3-17 p.

Baatz, M. and A. Schape, 2000. Multiresolution segmentation: an optimization approach for high quality multi-scale image segmentation., *Angewandte Geographische Informations-Verarbeitung XII* (J. Strobl, T. Blaschke and G. Griesebner, editors), Wichmann Verlag, Karlsruhe, pp. 12-23.

Beaulieu, J. M. and M. Goldberg, 1989. Hierarchy in picture segmentation - a stepwise optimization approach, *IEEE Transactions on Pattern Analysis and Machine Intelligence*, 11(2):150-163.

Benediktsson, J. A., M. Pesaresi and K. Arnason, 2003. Classification and feature extraction for remote sensing images from urban areas based on morphological transformations, *IEEE Transactions on Geoscience and Remote Sensing*, 41(9):1940-1949.

Benz, U., P. Hofmann, G. Willhauck, I. Lingenfelder and M. Heynen, 2004. Multi-resolution, object-oriented fuzzy analysis of remote sensing data for GIS-ready information, *ISPRS Journal of Photogrammetry and Remote Sensing*, 58(3-4):239-258.

Blaschke, T., C. Burnett and A. Pekkarinen, 2004. Image segmentation methods for object-based analysis and classification, *Remote sensing image analysis: including the sptial domain* (S.M.d. Jong and F.D.v.d. Meer, editors), Kluwer Academic Publishers, Dordrecht, Netherlands, pp. 211-223.

Breiman, L., J. Friedman, R. Olshen and C. J. Stone, 1984. *Classification and Regression Trees,* Chapman and Hall, New York, 146-150 p.

Carleer, A. and E. Wolff, 2004. Exploitation of very hight resolution satellite data for tree species identification, *Photogrammetric Engineering and Remote Sensing*, 70(1):135-140.

Clausi, D. A., 2002. An analysis of co-occurrence texture statistics as a function of grey level quantization, *Canadian Journal of Remote Sensing*, 28(1):45-62.

Czaplewski, R. L. and P. L. Patterson, 2003. Classification accuracy for stratification with remotely sensed data, *Forest Science*, 49(3):402-408.

Dennison, P. E. and D. A. Roberts, 2003. The effects of vegetation phenology on endmember selection and species mapping in southern California chaparral, *Remote Sensing of Environment*, 87(2-3):295-309.

Dymond, C. and E. Johnson, 2002. Mapping vegetation spatial patterns from modeled water, temperature and solar radiation gradients, *ISPRS Journal of Photogrammetry and Remote Sensing*, 57(1-2):69-85.

Ehlers, M., M. Gahler and R. Janowsky, 2003. Automated analysis of ultra high resolution remote sensing data for biotope type mapping: new possibilities and challenges, *ISPRS Journal of Photogrammetry and Remote Sensing*, 57(5-6):315-326.

Foody, G. M., 2002. Status of land cover classification accuracy assessment, *Remote Sensing of Environment*, 80(1):185-201.

Fu, K. S. and J. K. Mui, 1981. A survey on image segmentation, *Pattern Recognition*, 13(1):3-16.

Gambotto, J. P., 1993. A new approach to combining region growing and edge-detection, *Pattern Recognition Letters*, 14(11):869-875.

Gong, P., 1994. Reducing boundary effects in a kernel-based classifier, *International Journal of Remote Sensing*, 15(5):1131-1139.

Gong, P., 1996. Integrated analysis of spatial data from multiple sources: Using evidential reasoning and artificial neural network techniques for geological mapping, *Photogrammetric Engineering and Remote Sensing*, 62(5):513-523.

Gong, P. and P. J. Howarth, 1989. Performance analyses of probabilistic relaxation methods for land-cover classification, *Remote Sensing of Environment*, 30(1):33-42.

Gong, P. and P. J. Howarth, Year. Land cover to land use conversion: A knowledge-based approach, 18-23 March 1990, Denver, Colorado, ACSM-ASPRS Annual convention, 4:pp 447-456.

Gong, P. and P. J. Howarth, 1992a. Frequency-based contextual classification and gray-level vector reduction for land-use identification, *Photogrammetric Engineering and Remote Sensing*, 58(4):423-437.

Gong, P. and P. J. Howarth, 1992b. Land-use classification of SPOT HRV data using a cover-frequency method, *International Journal of Remote Sensing*, 13(8):1459-1471.

Gong, P., D. J. Marceau and P. J. Howarth, 1992. A comparison of spatial feature-extraction algorithms for land-use classification with SPOT HRV data, *Remote Sensing of Environment*, 40(2):137-151.

Gong, P., R. Pu and B. Yu, 1997. Conifer species recognition: An exploratory analysis of in situ hyperspectral data, *Remote Sensing of Environment*, 62(2):189-200.

Gong, P., R. Pu and B. Yu, 2001. Conifer species recognition: effects of data transformation, *International Journal of Remote Sensing*, 22(17):3471-3481.

Gould, W., 2000. Remote sensing of vegetation, plant species richness, and regional biodiversity hotspots, *Ecological Applications*, 10(6):1861-1870.

Hardin, P. J. and C. N. Thomson, 1992. Fast nearest neighbor classification methods for multispectral imagery, *Professional Geographer*, 44(2):191-202.

Harvey, K. R. and G. J. E. Hill, 2001. Vegetation mapping of a tropical freshwater swamp in the Northern Territory, Australia: a comparison of aerial photography, Landsat TM and SPOT satellite imagery, *International Journal of Remote Sensing*, 22(15):2911-2925.

Hay, G. J., D. J. Marceau, P. Dube and A. Bouchard, 2001. A multiscale framework for landscape analysis: Object-specific analysis and upscaling, *Landscape Ecology*, 16(6):471-490.

Hay, G. J., K. O. Niemann and G. F. McLean, 1996. An object-specific image texture analysis of H-resolution forest imagery, *Remote Sensing of Environment*, 55(2):108-122.

Heikkonen, J. and A. Varfis, 1998. Land cover land use classification of urban areas: A remote sensing approach, *International Journal of Pattern Recognition and Artificial Intelligence*, 12(4):475-489.

Herold, M., M. E. Gardner and D. A. Roberts, 2003a. Spectral resolution requirements for mapping urban areas, *IEEE Transactions on Geoscience and Remote Sensing*, 41(9):1907-1919.

Herold, M., X. H. Liu and K. C. Clarke, 2003b. Spatial metrics and image texture for mapping urban land use, *Photogrammetric Engineering and Remote Sensing*, 69(9):991-1001.

Hill, R. A., 1999. Image segmentation for humid tropical forest classification in Landsat TM data, *International Journal of Remote Sensing*, 20(5):1039-1044.

Hill, R. A. and G. M. Foody, 1994. Separability of tropical rain-forest types in the Tambopata-Candamo reserved zone, Peru, *International Journal of Remote Sensing*, 15(13):2687-2693.

Hodgson, M. E., 1998. What size window for image classification? A cognitive perspective, *Photogrammetric Engineering and Remote Sensing*, 64(8):797-807.

Hsieh, P. F., L. C. Lee and N. Y. Chen, 2001. Effect of spatial resolution on classification errors of pure and mixed pixels in remote sensing, *IEEE Transactions on Geoscience and Remote Sensing*, 39(12):2657-2663.

Jensen, J. R. and D. C. Cowen, 1999. Remote sensing of urban suburban infrastructure and socio-economic attributes, *Photogrammetric Engineering and Remote Sensing*, 65(5):611-622.

Johnsson, K., 1994. Segment-based land-use classification from SPOT satellite data, *Photogrammetric Engineering and Remote Sensing*, 60(1):47-53.

Kalliola, R. and K. Syrjanen, 1991. To what extent are vegetation types visible in satellite imagery, *Annales Botanici Fennici*, 28(1):45-57.

Kartikeyan, B., A. Sarkar and K. L. Majumder, 1998. A segmentation approach to classification of remote sensing imagery, *International Journal of Remote Sensing*, 19(9):1695-1709.

Keeler-Wolf, T., 1999. Field and photo-interpretation key to the vegetation alliances and defined associations from the Point Reyes National Seashore, Golden Gate National Recreation Area, San Francisco Municipal Water District Lands, and Mt. Tamalpais, Tomales Bay, and Samuel P. Taylor State Parks. Unpublished vegetation key.,

Kermad, C. D. and K. Chehdi, 2002. Automatic image segmentation system through iterative edge-region co-operation, *Image and Vision Computing*, 20(8):541-555.

Kettig, R. L. and D. A. Landgrebe, 1976. Classification of multispectral image data by extraction and classification of homogeneous objects, *IEEE Transactions on Geoscience and Remote Sensing*, 14(1):19-26.

Krishnaswamy, J., M. C. Kiran and K. N. Ganeshaiah, 2004. Tree model based eco-climatic vegetation classification and fuzzy mapping in diverse tropical deciduous ecosystems using multi-season NDVI, *International Journal of Remote Sensing*, 25(6):1185-1205.

Landgrebe, D. A., 1980. The development of a spectral - spatial classifier for earth observational data, *Pattern Recognition*, 12(3):165-175.

Lemoigne, J. and J. C. Tilton, 1995. Refining image segmentation by integration of edge and region data, *IEEE Transactions on Geoscience and Remote Sensing*, 33(3):605-615.

Lutes, J., 2002. DAIS: A digital airborne imaging system,

http://www.spaceimaging.com/products/dais/index.htm, Space Imaging, Inc.

Marceau, D. J., P. J. Howarth, J. M. M. Dubois and D. J. Gratton, 1990. Evaluation of the gray-level cooccurrence matrix-method for land-cover classification using SPOT imagery, *IEEE Transactions on Geoscience and Remote Sensing*, 28(4):513-519.

McIver, D. K. and M. A. Friedl, 2002. Using prior probabilities in decision-tree classification of remotely sensed data, *Remote Sensing of Environment*, 81(2-3):253-261.

Mehnert, A. and P. Jackway, 1997. An improved seeded region growing algorithm, *Pattern Recognition Letters*, 18(10):1065-1071.

Qi, Z., 1996. Extraction of spectral reflectance images from multi-spectral images by the HIS transformation model, *International Journal of Remote Sensing*, 17(17):3467-3475.

Qin, Z., A. Karnieli and P. Berliner, 2001. A mono-window algorithm for retrieving land surface temperature from Landsat TM data and its application to the Israel-Egypt border region, *International Journal of Remote Sensing*, 22(18):3719-3746.

Richards, J. A. and X. Jia, 1999. *Remote sensing digital image analysis,* Springer, New York, 225-228 p.

San Miguel-Ayanz, J. and G. S. Biging, 1996. An iterative classification approach for mapping natural resources from satellite imagery, *International Journal of Remote Sensing*, 17(5):957-981.

Sandmann, H. and K. P. Lertzman, 2003. Combining high-resolution aerial photography with gradient-directed transects to guide field sampling and forest mapping in mountainous terrain, *Forest Science*, 49(3):429-443.

Shackelford, A. K. and C. H. Davis, 2003. A hierarchical fuzzy classification approach for high-resolution multispectral data over urban areas, *IEEE Transactions on Geoscience and Remote Sensing*, 41(9):1920-1932.

Srinivasan, A. and J. A. Richards, 1990. Knowledge-based techniques for multisource classification, *International Journal of Remote Sensing*, 11(3):505-525.

Steele, B. M., J. C. Winne and R. L. Redmond, 1998. Estimation and mapping of misclassification probabilities for thematic land cover maps, *Remote Sensing of Environment*, 66(2):192-202.

Sun, W. X., V. Heidt, P. Gong and G. Xu, 2003. Information fusion for rural land-use classification with high-resolution satellite imagery, *IEEE Transactions on Geoscience and Remote Sensing*, 41(4):883-890.

Ton, J. C., J. Sticklen and A. K. Jain, 1991. Knowledge-based segmentation of landsat images, *IEEE Transactions on Geoscience and Remote Sensing*, 29(2):222-232.

APPENDIX A: Classification System

	Class number	alliance code	Class name	Alliance	*Latin name*
Forest	1	1010	California Bay	California Bay	*Umbellularia californica*
	2	1030	Eucalyptus	Eucalyptus	*Eucalyptus spp.*
	3	1070	Tanoak	Tanoak	*Lithocarpus densiflora*
	4	1090	Giant Chinquapin	Giant Chinquapin	*Chrysolepis chrysophylla*
	5	2010	Douglas fir	Douglas fir	*Pseudotsuga menziesii*
	6	2050	Coast redwood	Coast redwood	*Sequoia sempervirens*
	7	3030	Bishop pine	Bishop pine	*Pinus muricata*
	8	3120	Monterey cypress/pine	Monterey cypress/pine	*Cupressus macrocarpa/Pinus radiata*
	9	7060	Willow Mapping Unit	Yellow willow	*Salix lutea*
				Black willow	*Salix nigra*
				Red willow	*Salix laevigata*
	10	7070	Red Alder	Red Alder	*Alnus rubra*
	11	12020	Coast Live Oak	Coast Live Oak	*Quercus agrifolia*
	12	14020	California Buckeye	California Buckeye	*Aesculus californica*
Shrub	13	19010	Yellow bush lupine	Yellow bush lupine	*Lupinus arboreus*
	14	20010	California Wax Myrtle	California Wax Myrtle	*Myrica californica*
	15	20020	Blue blossom	Blue blossom	*Ceanothus thyrsiflorus*
	16	21110	Chamise	Chamise	*Adenostoma fasciculatum*
	17	21210	Eastwood Manzanita	Eastwood Manzamita	*Arctostaphylos glandulosa*
	18	21460	Coffeeberry	Coffeeberry	*Rhamnus californica*
	19	21470	Mixed Manzanita	Mixed Manzanita	*Arctostaphylos manzanita*
	20	21480	Sensitive manzanita	Sensitive manzanita	*Arctostaphylos nummularia*
	21	24040	Mixed Broom	Mixed Broom	*Cytisus spp., Spartium spp.,Genista spp.*
	22	24050	Coyote Brush	Coyote Brush	*Baccharis pilularis*
	23	24080	California Sagebrush	California Sagebrush	*Artemisia californica*
	24	24999	Gorse	Gorse	*Ulex europea*
	25	30010	Hazel	Hazel	*Corylus cornuta*
	26	30040	Poison Oak	Poison Oak	*Toxicodendron diversilobum*
	27	30050	Salmonberry	Salmonberry	*Rubus spectabilis*
	28	32080	Arroyo Willow	Arroyo Willow	*Salix lasiolepis*
	29	46020	Pacific Reedgrass	Pacific Reedgrass	*Calamagrostis nutkaensis*
Herb	30	47010	European Dunegrass	European Dunegrass	*Ammophila arenaria*
	31	47030	Perennial Grasslands	Perennial Grasslands	
	32	51010	Saltgrass	Saltgrass	*Distichlis spicata*
	33	52030	Rush	Rush	*Juncus effusus*
	34	52040	Tufted Hairgrass	Tufted Hairgrass	*Deschampsia caespitosa*
	35	55020	Bulrush-cattail spikerush	Bulrush-cattail spikerush	*Scirpus spp.-Typha spp.-Eleocharis spp.*
	36	56010	Cordgrass	Cordgrass	*Spartina foliosa*
	37	62040	Iceplant	Iceplant	*Carpobrotus edulus*
	38	62050	Coast Buckwheat	Coast Buckwheat	*Eriogonum latifolium*
	39	62060	Dune sagebrush-goldenbush	Dune sagebrush-goldenbush	*Artemisia pycnocephala-Isocoma menziesii*
	40	64030	Pickleweed	Pickleweed	*Salicornia spp.*

	41	67010	California annual grassland weedy	California annual grassland weedy	
	42	67020	California annual grassland	California annual grassland	
	43	67030	Purple Needlegrass	Purple Needlegrass	*Nassella pulchra*
Others	44	90300	Urban		
	45	90400	Non-vegatated		
	46	90401	Dune		
	47	90402	Beaches		
	48	98000	Water		

APPENDIX B: Confusion matrix for object-based 1-NN and pixel-based MLC

Object-based 1-NN

- Forest (%)

Class number	Number of objects	1	2	3	4	5	6	7	8	9	10	11	12
01	640	0.51	0.02	0.07	0.20	0.16	0.11	0.13	0.15	0.16	0.21	0.28	0.23
02	93	0.00	0.70	0.00	0.00	0.00	0.00	0.01	0.01	0.01	0.02	0.02	0.00
03	27	0.00	0.00	0.52	0.00	0.02	0.02	0.00	0.00	0.00	0.00	0.00	0.00
04	30	0.01	0.00	0.00	0.23	0.00	0.00	0.02	0.00	0.02	0.01	0.00	0.00
05	675	0.15	0.02	0.30	0.17	0.61	0.19	0.09	0.06	0.03	0.06	0.08	0.09
06	190	0.04	0.00	0.11	0.00	0.03	0.62	0.01	0.00	0.01	0.01	0.04	0.00
07	398	0.08	0.03	0.00	0.23	0.07	0.02	0.65	0.01	0.04	0.04	0.02	0.09
08	85	0.02	0.02	0.00	0.00	0.01	0.01	0.00	0.42	0.08	0.04	0.01	0.00
09	158	0.02	0.08	0.00	0.07	0.01	0.01	0.02	0.06	0.36	0.12	0.06	0.09
10	339	0.09	0.09	0.00	0.03	0.04	0.02	0.04	0.22	0.20	0.40	0.07	0.18
11	176	0.07	0.02	0.00	0.07	0.04	0.02	0.03	0.04	0.09	0.05	0.41	0.09
12	22	0.01	0.02	0.00	0.00	0.00	0.00	0.01	0.02	0.01	0.02	0.01	0.23
accuracy		0.51	0.70	0.52	0.23	0.61	0.62	0.65	0.42	0.36	0.40	0.41	0.23

- Shrub (%)

Class number	Number of objects	13	14	15	16	17	18	19	20	21	22	23	24	25	26	27	28	29
13	61	0.48	0.00	0.02	0.00	0.00	0.00	0.00	0.00	0.00	0.01	0.02	0.05	0.00	0.02	0.02	0.02	0.02
14	97	0.03	0.24	0.02	0.00	0.00	0.00	0.00	0.00	0.02	0.03	0.00	0.05	0.00	0.04	0.03	0.08	0.13
15	133	0.03	0.01	0.56	0.00	0.00	0.10	0.05	0.00	0.04	0.04	0.00	0.05	0.00	0.04	0.06	0.03	0.01
16	66	0.00	0.00	0.00	0.59	0.31	0.00	0.10	0.03	0.00	0.01	0.00	0.00	0.06	0.00	0.00	0.00	0.00
17	42	0.00	0.00	0.00	0.17	0.26	0.00	0.15	0.24	0.00	0.00	0.00	0.00	0.00	0.00	0.00	0.00	0.00
18	40	0.00	0.02	0.02	0.02	0.00	0.23	0.03	0.00	0.02	0.01	0.00	0.00	0.06	0.04	0.00	0.00	0.00
19	39	0.00	0.00	0.00	0.08	0.14	0.00	0.56	0.14	0.02	0.00	0.00	0.00	0.00	0.00	0.00	0.00	0.00
20	29	0.00	0.00	0.00	0.03	0.29	0.00	0.05	0.52	0.00	0.00	0.00	0.00	0.06	0.00	0.00	0.00	0.00
21	100	0.00	0.00	0.03	0.00	0.00	0.08	0.03	0.00	0.65	0.02	0.00	0.00	0.00	0.00	0.00	0.01	0.00
22	1158	0.20	0.42	0.31	0.11	0.00	0.50	0.03	0.07	0.25	0.75	0.53	0.45	0.29	0.57	0.37	0.26	0.18
23	45	0.05	0.00	0.00	0.00	0.00	0.00	0.00	0.00	0.00	0.01	0.33	0.05	0.00	0.00	0.00	0.00	0.00
24	20	0.05	0.00	0.00	0.00	0.00	0.00	0.00	0.00	0.00	0.01	0.04	0.10	0.00	0.00	0.02	0.01	0.01
25	17	0.00	0.00	0.00	0.00	0.00	0.03	0.00	0.00	0.00	0.00	0.00	0.00	0.47	0.00	0.02	0.00	0.00
26	49	0.03	0.00	0.01	0.00	0.00	0.08	0.00	0.00	0.00	0.02	0.04	0.00	0.00	0.16	0.03	0.02	0.01
27	63	0.00	0.03	0.02	0.02	0.00	0.00	0.00	0.00	0.00	0.02	0.02	0.05	0.06	0.04	0.27	0.04	0.00
28	159	0.07	0.04	0.02	0.00	0.00	0.00	0.00	0.00	0.00	0.03	0.00	0.10	0.00	0.06	0.13	0.39	0.10
29	176	0.07	0.24	0.02	0.00	0.00	0.00	0.00	0.00	0.00	0.03	0.00	0.10	0.00	0.02	0.06	0.14	0.55
accuracy		0.48	0.24	0.56	0.59	0.26	0.23	0.56	0.52	0.65	0.75	0.33	0.10	0.47	0.16	0.27	0.39	0.55

- Herb (%)

Class number	Number of objects	30	31	32	33	34	35	36	37	38	39	40	41	42	43
30	63	0.46	0.00	0.02	0.05	0.00	0.02	0.00	0.03	0.00	0.04	0.01	0.00	0.00	0.00
31	248	0.10	0.56	0.08	0.10	0.07	0.05	0.00	0.06	0.00	0.07	0.07	0.11	0.09	0.00
32	101	0.03	0.01	0.34	0.02	0.04	0.15	0.07	0.01	0.00	0.01	0.10	0.01	0.00	0.00
33	508	0.33	0.24	0.25	0.63	0.25	0.34	0.00	0.33	0.00	0.30	0.25	0.06	0.09	0.00
34	28	0.00	0.02	0.00	0.01	0.50	0.02	0.00	0.00	0.00	0.00	0.00	0.01	0.01	0.00
35	59	0.03	0.01	0.08	0.04	0.04	0.31	0.00	0.01	0.00	0.01	0.04	0.06	0.00	0.00
36	14	0.00	0.00	0.02	0.00	0.00	0.00	0.64	0.00	0.00	0.00	0.05	0.00	0.00	0.00
37	100	0.02	0.02	0.02	0.04	0.00	0.00	0.00	0.43	0.00	0.10	0.03	0.01	0.00	0.00
38	5	0.00	0.00	0.00	0.00	0.00	0.00	0.00	0.00	1.00	0.00	0.00	0.00	0.00	0.00
39	67	0.03	0.02	0.00	0.05	0.00	0.02	0.00	0.07	0.00	0.40	0.01	0.02	0.02	0.00
40	177	0.00	0.05	0.15	0.05	0.04	0.07	0.29	0.04	0.00	0.03	0.37	0.08	0.00	0.00
41	109	0.00	0.03	0.05	0.01	0.07	0.02	0.00	0.02	0.00	0.01	0.06	0.57	0.16	0.29
42	93	0.00	0.03	0.00	0.01	0.00	0.02	0.00	0.00	0.00	0.00	0.01	0.07	0.62	0.00
43	7	0.00	0.00	0.00	0.00	0.00	0.00	0.00	0.00	0.00	0.00	0.00	0.00	0.01	0.71
accuracy		0.46	0.56	0.34	0.63	0.50	0.31	0.64	0.43	1.00	0.40	0.37	0.57	0.62	0.71

- Others (%)

Class number	Number of objects	44	45	46	47	48
44	94	0.95	0.23	0.05	0.07	0.02
45	13	0.01	0.69	0.00	0.05	0.02
46	21	0.01	0.00	0.76	0.05	0.00
47	41	0.03	0.08	0.19	0.80	0.06
48	48	0.00	0.00	0.00	0.02	0.90
accuracy		0.95	0.69	0.76	0.80	0.90

* The accuracies listed above are different from table 4. Here the confusion matrix is object-based. The accuracies in table 4 are pixel-based accuracies, which are actually from those object-based confusion matrix weighted by the area of objects.

Pixel-based MLC

- Forest (%)

Class number	Number of pixels	1	2	3	4	5	6	7	8	9	10	11	12
01	2244919	19.71	1.66	7.5	5.26	11.14	16.12	9.44	2.32	6.49	3.59	6	10.75
02	275417	0.85	70.65	0.03	1.55	4.6	0.91	1.63	6.58	3.68	1.52	2.4	5.6
03	91319	4.58	0.2	76.99	2.04	3.06	10.64	0.22	0.09	0.31	0.25	1.47	0.16
04	159485	1.48	2.12	0.75	63.01	0.39	9.6	8.71	1.17	6.68	1.94	3.9	0.26
05	2780024	6.06	1.68	20.71	1.97	26.66	19.46	1.96	8.28	4.91	2.59	3.42	2.3
06	713850	6.22	0.22	14.4	1.48	4.59	65.92	0.22	0.24	0.44	0.26	4.31	1.71
07	1900420	3.64	4.46	0.3	13.77	3.12	1.44	55.36	1.02	9.72	3.36	2.08	1.73
08	288460	1.13	4.65	2.11	1.63	11.19	4.21	2.62	55.67	6.64	2.13	3.76	4.26
09	540822	1.88	5.44	2.63	8.74	5.75	2.16	3.56	8.24	44.74	7.79	4.11	4.97
10	1143740	3.97	5.94	2.33	7.94	10.21	4.66	14.49	7.62	22.48	12.2	3.49	4.66
11	587606	7.69	4.88	2.07	4.92	13.23	16.61	7.82	9.37	4.88	2.54	18.76	7.23
12	56487	4.35	0.66	0.06	0.49	2.03	2.74	0.12	0.88	2.93	1.84	0.74	83.15
accuracy		19.71	70.65	76.99	63.01	26.66	65.92	55.36	55.67	44.74	12.2	18.76	83.15

- Shrub (%)

Class number	Number of pixels	13	14	15	16	17	18	19	20	21	22	23	24	25	26	27	28	29
13	187250	73.36	0.88	0.54	0.07	0	0.28	0	0	0.15	2.94	7.19	0.62	0.35	4.98	5.72	1.65	1.26
14	312800	2.54	54.84	1.61	0.1	0	1.66	0.02	0	3.89	4.2	1.1	0.06	1.2	3.94	7.97	4.56	12.32
15	775670	2.38	0.53	63.72	2.84	0.01	4.49	0.47	0.04	1.1	8.17	1.05	0	1.42	9.03	2.63	2	0.11
16	294800	0.27	0.15	1.59	74.94	0.28	1.42	7.97	0.06	1.91	2.66	1.31	0	3.92	2.9	0.15	0.45	0.01
17	180892	0.02	0.01	0.07	1.89	71.16	0.02	3.34	20.49	0.03	0.82	0	0	1.44	0.53	0.17	0	0
18	164739	2.06	0.26	14.03	3.65	0	61.43	0.26	0.03	1.7	4.06	1.65	0	1.86	3.8	0.13	0.42	4.67
19	229896	0.01	0.22	0.07	4.43	10.69	0.75	64.01	13.65	0.56	1.94	0	0	2.72	0.41	0.52	0	0
20	193232	0.02	0.05	0.14	1.51	26.2	0.48	5.81	60.45	1.09	1.18	0	0	2.49	0.41	0.16	0	0
21	424961	0.34	0.2	2.01	2.09	0	2.42	5.71	0.21	75.43	2.34	2.11	0.03	2.5	3.1	0.17	1.3	0.03
22	7274633	7.56	5.65	11.14	1.36	0.13	2.13	0.83	0.05	2.89	27.37	11.3	0.42	1.49	9.4	8.48	4.31	5.42
23	168132	3.09	0.04	1.08	0.19	0	0.09	0.05	0	1.18	4.98	83.2	0.23	0.28	3.61	0.15	1.81	0.01
24	97903	2.54	5.18	0.19	0.02	0	0.01	0	0	0.13	1.83	1.36	75.11	0.79	0.82	2.13	7.2	2.69
25	92010	0.02	0	0.09	0.83	0.12	0.86	1.67	1.32	0.02	0.38	0	0	93.97	0.31	0.41	0	0
26	287856	7.86	1.97	3.89	0.61	0.02	7.06	0.53	0	2.96	4.69	5.6	0.68	2.19	51.94	5.39	2.65	1.96
27	237207	3.65	3.49	5.72	0.27	0.09	0.24	0.12	0.02	0.09	6.26	0.01	0.24	1.85	7.18	60.29	6.91	3.56
28	669850	8.78	5.13	4.13	0.24	0	2.16	0.13	0	2.58	5.38	3.16	3.35	0.69	10.02	9.47	32.92	11.83
29	867911	4.43	9.71	0.5	0.02	0	0.05	0.01	0	1.21	2.16	0.57	0.33	0.44	1.63	8.75	7.26	62.94
accuracy		73.36	54.84	63.72	74.94	71.16	61.43	64.01	60.45	75.43	27.37	83.2	75.11	93.97	51.94	60.29	32.92	62.94

- Herb (%)

Class number	Number of pixels	30	31	32	33	34	35	36	37	38	39	40	41	42	43
30	223477	65.33	1.1	1	9.32	1.03	4.49	0	5.27	0	10.63	0	1.12	0.73	0
31	1528375	2.48	32.24	1.22	10.39	5.44	15.73	0	3.88	0.01	2.46	1.05	7.5	17.61	0.01
32	351222	1.18	2.87	28.32	5.57	0.13	16.98	1.11	2.22	0.26	0.48	34.7	3.08	3.12	0
33	2651710	16.53	12.25	3.03	24.89	6.63	11.9	0	8.1	0.02	2.51	1.02	6.05	7.07	0
34	113681	0.12	0.81	0.07	2.43	86.11	1.2	0	1.19	0	0.15	1.13	6.01	0.78	0
35	326175	3.13	4.29	6.12	2.26	0.38	67.8	0	1.27	0	0.84	9.83	0.99	3.08	0
36	104303	0	0.01	1.49	0	0	0.02	70.58	0	0	0	27.66	0.24	0	0
37	326366	9.76	5.45	1.5	9.79	6.55	5.27	0	51.98	0	1.77	2.14	3.78	2.01	0
38	51004	0	0.26	0.47	0.38	0	0	0	0.14	97.17	0	0.51	0.83	0.24	0
39	257989	21.78	5.28	2.63	16.44	1.18	3.71	0	13.24	0	33.66	0.37	1.16	0.54	0
40	922398	0.3	1.84	6.15	1.95	0.56	7.68	7.27	1.98	0	0.17	68.76	1.87	1.47	0
41	598730	0.24	10.24	1.38	3.38	10.85	4.55	0.03	2.94	0.04	0.75	2.03	39.75	23.8	0
42	533223	0.37	3.65	1.1	2.35	1.14	1.22	0	1.02	0	0.57	1.55	10.93	76.11	0
43	22180	0	0.37	0	0	0	0	0	0	0	0	0	17.95	7	74.68
accuracy		65.33	32.24	28.32	24.89	86.11	67.8	70.58	51.98	97.17	33.66	68.76	39.75	76.11	74.68

- Others (%)

Class number	Number of pixels	44	45	46	47	48
44	145647	92.76	6.21	0.15	0.81	0.08
45	16049	8.19	91.28	0	0.45	0.07
46	57039	1.79	0	98.03	0.18	0
47	184629	4.75	0.03	0	94.76	0.46
48	823981	0.44	0	0.21	6.45	92.9
accuracy		92.76	91.28	98.03	94.76	92.9

APPENDIX C: Project delivery list and metadata

1. Vegetation map from classification in shape file

The polygon is the classification object from segmentation in eCognition. We list the first three classes and their membership values in the attribute table.

Refer to page 42 for the definition of membership value.

2. Training samples in shape file

The training samples are derived from NPS vegetation database.

3. Topography data in ESRI GRID file

DEM: 10 m resolution

Distance to watercourses : 10 m resolution

4. Project technical report in PDF